Title

Protein Kinase C Quality Control by Phosphatase PHLPP1 Unveils Loss-of-Function Mechanism in Cancer

Journal

Molecular Cell, 74(2)

ISSN

1097-2765

Authors

Baffi, Timothy R
Van, An-Angela N
Zhao, Wei
et al.

Publication Date

2019-04-01

DOI

10.1016/j.molcel.2019.02.018

Peer reviewed

HHS Public Access

Author manuscript

Mol Cell. Author manuscript; available in PMC 2020 April 18.

Published in final edited form as:

Mol Cell. 2019 April 18; 74(2): 378–392.e5. doi:10.1016/j.molcel.2019.02.018.

Protein Kinase C Quality Control by Phosphatase PHLPP1 Unveils Loss-of-Function Mechanism in Cancer

Timothy R. Baffi[1,2], **An-Angela N. Van**[1,2], **Wei Zhao**[3], **Gordon B. Mills**[3], and **Alexandra C. Newton**[*,1]

[1]Department of Pharmacology, University of California at San Diego, La Jolla, CA 92093, USA

[2]Biomedical Sciences Graduate Program, University of California at San Diego, La Jolla, CA 92093, USA

[3]Department of Systems Biology, The University of Texas MD Anderson Cancer Center, Houston, TX 77030, USA

Graphical Abstarct

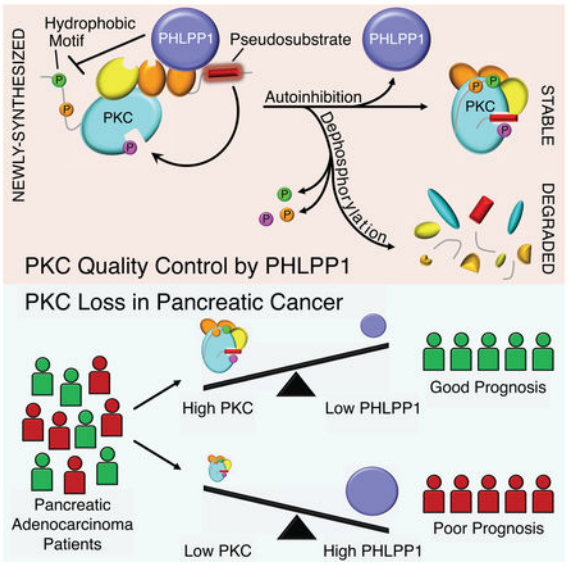

SUMMARY

Protein kinase C (PKC) isozymes function as tumor suppressors in increasing contexts. In contrast to oncogenic kinases whose function is acutely regulated by transient phosphorylation, PKC is

*Correspondence: anewton@ucsd.edu.

AUTHOR CONTRIBUTIONS

TRB and ACN conceived the project and designed the experiments. TRB and ANV performed the experiments. WZ performed the tumor profiling under the mentorship of GBM. TRB and ACN wrote the manuscript.

DECLARATION OF INTERESTS

The authors declare no conflict of interest with the contents of this article.

constitutively phosphorylated following biosynthesis to yield a stable, autoinhibited enzyme that is reversibly activated by second messengers. Here we report that the phosphatase PHLPP1 opposes PKC phosphorylation during maturation, leading to the degradation of aberrantly active species that do not become autoinhibited. Cancer-associated hotspot mutations in the pseudosubstrate of PKCβ that impair autoinhibition result in dephosphorylated and unstable enzymes. Protein-level analysis reveals that PKCα is fully phosphorylated at the PHLPP site in over 5000 patient tumors, with higher PKC levels correlating (1) inversely with PHLPP1 levels and (2) positively with improved survival in pancreatic adenocarcinoma. Thus, PHLPP1 provides a proofreading step that maintains the fidelity of PKC autoinhibition and reveals a prominent loss-of-function mechanism in cancer by suppressing the steady-state levels of PKC.

eTOC Blurb

PKC generally functions as a tumor suppressor. Baffi et al. uncover a quality control mechanism in which PHLPP1 opposes priming phosphorylation of newly-synthesized PKC to suppress its steady-state levels. This quality control dominates in pancreatic cancer: patients with high levels of PKC and low levels of PHLPP1 have improved survival.

Keywords

protein kinase C; PHLPP1; phosphorylation; degradation; cancer; loss-of-function; autoinhibition; quality control

INTRODUCTION

Cellular homeostasis depends on exquisite regulation of protein kinase and phosphatase activity to allow precise responses to extracellular signals (Brognard and Hunter, 2011). Deregulation of phosphorylation mechanisms is a hallmark of disease, with aberrant kinase and phosphatase activity driving an abundance of pathologies. One kinase family whose activity must be precisely tuned to avoid pathophysiologies is protein kinase C (PKC).

PKC family members transduce myriad signals downstream of phospholipid hydrolysis to regulate diverse cellular functions such as proliferation, apoptosis, migration, and differentiation (Griner and Kazanietz, 2007; Newton, 2018). Although assumed to be oncoproteins for decades, analysis of cancer-associated mutations and protein expression levels support a general tumor-suppressive role for PKC isozymes, accounting for the failure, and in some cases worsened patient outcome, of PKC inhibitors in cancer clinical trials (Antal et al., 2015b; Zhang et al., 2015). Conversely, enhanced activity is associated with degenerative diseases such as Alzheimer's disease, spinocerebellar ataxia, and increased risk of cerebral infarction (Newton, 2018). Even small changes in PKC activity drive pathogenesis, as illustrated by a germline mutation in affected family members with Alzheimer's disease that causes a modest 30% increase in the catalytic rate of the enzyme (Callender et al., 2018). Thus, tight regulation of PKC signaling output is essential.

PKC isozymes are multi-domain Ser/Thr kinases whose activity is governed by reversible release of an autoinhibitory pseudosubstrate segment (Newton, 2018). For conventional PKC

(cPKC) isozymes (Figure 1A; α, β, γ), this is controlled by binding of the lipid second messenger diacylglycerol (DAG) to the second of two tandem C1 domains. Ca^{2+} binding to a plasma membrane-directing C2 domain facilitates activation of these isozymes by localizing them on the membrane, thereby increasing the probability of binding DAG. Engaging both the C2 and C1B domains on membranes provides the energy to release the pseudosubstrate, allowing substrate phosphorylation and downstream signaling. This activation is short-lived, with the enzyme reverting to the autoinhibited conformation upon return of Ca^{2+} and DAG to unstimulated levels.

Like many kinases, PKC is also regulated by phosphorylation. However, unlike many kinases, these phosphorylations occur shortly after biosynthesis and are constitutive (Borner et al., 1989; Keranen et al., 1995). Newly-synthesized conventional PKC is matured by phosphorylation at three conserved positions: the activation loop by the phosphoinositide-dependent kinase PDK-1 (Dutil et al., 1998; Le Good et al., 1998) and two C-terminal sites, the turn and hydrophobic motifs (Keranen et al., 1995). The C-tail phosphorylations depend upon both the kinase complex mammalian Target of Rapamycin complex 2 (mTORC2) (Guertin et al., 2006) and the intrinsic catalytic activity of PKC, with *in vitro* studies showing that PKC autophosphorylates by an intramolecular reaction at the hydrophobic motif (Behn-Krappa and Newton, 1999).

Mechanisms that prevent the phosphorylation of PKC, such as loss of PDK-1, inhibition of mTORC2, or impairing the catalytic activity of PKC, result in PKC degradation (Balendran et al., 2000; Guertin et al., 2006; Hansra et al., 1999). Indeed, it is this sensitivity of the unphosphorylated species to degradation that accounts for the ability of phorbol esters, potent PKC agonists, to cause the “down-regulation” of PKC (Jaken et al., 1981). The membrane-engaged active conformation of PKC is highly sensitive to dephosphorylation (Dutil et al., 1994), and dephosphorylation at the hydrophobic motif by the PH domain Leucine-rich repeat Protein Phosphatase (PHLPP) serves as the first step in the degradation of PKC, triggering subsequent PP2A-dependent dephosphorylation at the turn motif and activation loop (Gao et al., 2008; Hansra et al., 1999; Lu et al., 1998). Thus, PKC signaling output is regulated not only by second messengers, but also by mechanisms that establish the level of PKC protein in the cell. Understanding how to modulate these levels has important therapeutic implications as high PKC levels correlate with improved survival in diverse cancers (Newton, 2018).

Here we report a quality control mechanism in which PHLPP1 ensures the fidelity of PKC maturation by proofreading the conformation of newly-synthesized PKC. Specifically, phosphorylation of the hydrophobic motif is necessary to adopt an autoinhibited conformation, and this autoinhibited conformation then protects the hydrophobic motif from dephosphorylation by PHLPP1, thus protecting PKC from degradation. In cancer, hotspot mutations in the pseudosubstrate are loss-of-function (LOF) because of this proofreading mechanism. The ratio of hydrophobic motif phosphorylation to total PKCα in over 5,000 tumor samples reveals a near 1:1 ratio, validating mechanistic studies showing that if PKC is not phosphorylated at the hydrophobic motif, it is degraded. Finally, high levels of PKC hydrophobic motif phosphorylation (and hence total PKC) correlate inversely with PHLPP1 levels and co-segregate with improved patient survival in pancreatic adenocarcinoma,

implicating PKC phosphorylation as both a prognostic marker and therapeutic target. This PHLPP1-dependent quality control mechanism provides a general LOF mechanism for a tumor suppressor in cancer by targeting post-translational modifications.

RESULTS

PKC Priming Phosphorylations are Necessary for Maturation and Activity

PKC priming phosphorylations (Figure 1A, 1B) have been presumed to be necessary for catalytic competence based on biochemical studies (Bornancin and Parker, 1997; Cazaubon et al., 1994; Edwards and Newton, 1997; Orr and Newton, 1994). To assess whether phosphorylation at these sites is also necessary in a cellular context, we measured the agonist-evoked activity of wild-type (WT) PKCβII or mutants with non-phosphorylatable residues at each of the three priming sites in cells using the C Kinase Activity Reporter (CKAR) (Violin et al., 2003). PDBu treatment caused a robust increase in CKAR phosphorylation in COS7 cells expressing WT PKC or turn motif mutant (T641A) that was reversed by addition of PKC inhibitor (Figure 1C). In contrast, cells expressing activation loop (T500V) or hydrophobic motif (S660A) mutants displayed no increase in CKAR phosphorylation above that of endogenous PKC. Thus, phosphorylatable residues at the activation loop and hydrophobic motif, but not turn motif, are necessary for cellular PKC activity. Western blot analysis with phospho-specific antibodies revealed that WT PKCβII protein was phosphorylated at the C-terminal sites (causing an electrophoretic mobility shift (asterisk) (Keranen et al., 1995)) and at the activation loop (Figure 1D). The T641A protein was phosphorylated at the activation loop and hydrophobic motif, whereas the T500V and S660A proteins were unphosphorylated at all three sites, exhibited by their faster mobility (dash) and lack of reactivity with phospho-specific antibodies (Figure 1D). To assess whether negative charge at the hydrophobic motif is sufficient for cellular PKC activity, we examined the PDBu-stimulated activity of phosphomimetic PKC mutants with Glu substitutions at either or both of the C-tail phosphorylation sites (Figure 1E). Replacement with Glu at the turn motif (T641E), hydrophobic motif (S660E), or both C-terminal sites (T641E/S660E) resulted in comparable activation kinetics as those observed with WT PKCβII (see Figure 1C). In contrast, PKCβII T641E/S660A was inactive, revealing a requirement for negative charge at the hydrophobic motif irrespective of turn motif phosphorylation. Thus, phosphorylation of the activation loop and hydrophobic motif, but not the turn motif, is necessary for PKC maturation and enzymatic activity in cells.

The Autoinhibitory Pseudosubstrate is Required for Cellular PKC Phosphorylation

Extensive *in vitro* biochemical studies have established that the pseudosubstrate is necessary to restrain PKC activity in the absence of second messengers (House and Kemp, 1987; Orr et al., 1992; Pears et al., 1990). To probe the role of the pseudosubstrate in a cellular context, we deleted the 18 amino acid pseudosubstrate segment of two cPKC isozymes, PKCα and PKCβII (Figure 2A; PKCα ΔPS and PKCβII ΔPS), and examined the phosphorylation state and cellular activity of the expressed proteins. Deletion of the pseudosubstrate abolished phosphorylation at all three priming sites (Figure 2B), which could not be rescued by treatment with the phosphatase inhibitor Calyculin A (Figure S1). Surprisingly, however, analysis of PKC basal activity, assessed by the drop in CKAR phosphorylation upon

addition of PKC inhibitor, revealed that PKCβII ΔPS had high basal activity despite the absence of priming phosphorylations (Figure 2C). Whereas both WT PKCα and PKCβII were activated by treatment of cells with UTP and PDBu, neither PKCα ΔPS nor PKCβII ΔPS responded to either agonist, but constitutive, maximal activity was revealed upon inhibitor addition (Figure 2D, 2E). Thus, deletion of the pseudosubstrate results in constitutively active PKC that, unexpectedly, has maximal activity in the absence of priming phosphorylations.

Given that replacement of the hydrophobic motif Ser with Ala abolished cellular PKC activity (Figure 1C), we used phosphorylation mutants of PKCβII ΔPS (which is not phosphorylated and constitutively active) to assess whether negative charge at the hydrophobic motif is required in the maturation of PKC but becomes dispensable thereafter. Turn motif mutants PKCβII ΔPS T641A and PKCβII ΔPS T641E had enhanced basal activity with little preference for Ala vs Glu (Figure 2F). In contrast, only the phosphomimetic Glu, but not Ala or Asn, at the hydrophobic motif site had activity (Figure 2G). Mutation of the hydrophobic motif did not simply alter substrate specificity to abolish recognition of CKAR: Western blot analysis using a phospho-Ser PKC substrate antibody revealed no significant phosphorylation above basal levels in cells expressing PKCβII ΔPS S660A but robust phosphorylation in cells expressing PKCβII ΔPS (Figure S2). These data reveal that deletion of the pseudosubstrate (1) results in a constitutively active PKC that retains no phosphorylation at the priming sites and (2) does not bypass the requirement for negative charge at the hydrophobic motif to gain catalytic competence.

The Autoinhibited Conformation of PKC Retains Priming Phosphorylations

To explore the relationship between PKC phosphorylation and activity, we used a PKC conformation reporter, Kinameleon, wherein intramolecular rearrangements within PKC alter FRET between flanking CFP and YFP molecules (Figure 3A). Using this reporter, we previously showed that PKC adopts at least three distinct conformations: (1) a low FRET unprimed state, in which the regulatory domains are exposed; (2) an intermediate FRET primed state, in which PKC is fully phosphorylated at the C-terminal sites and autoinhibited, with the regulatory domains masked; and (3) a high FRET active state, in which the regulatory domains are engaged on the plasma membrane (Figure 3A) (Antal et al., 2014). To examine how autoinhibition affects PKC conformation, we altered the affinity of the pseudosubstrate for the kinase domain by either scrambling the position of positively charged amino acids in the pseudosubstrate (Figure 3B; Scrambled Mutant) or replacing them with neutral residues (Figure 3B; Neutral Mutant) in the Kinameleon reporter. Analysis of basal FRET, indicative of the average conformation of the PKC embedded in the reporter, revealed that the scrambled PKCβII Scram PS) and neutral PKCβII Neu PS) pseudosubstrate mutants had significantly lower basal FRET ratios than WT PKCβII, consistent with an unprimed, open conformation (Figure 3C). However, the scrambled mutant displayed modest propensity to autoinhibit, as introduction of a kinase-dead mutation in PKCβII Scram PS (Scram PS K371R, which abolishes hydrophobic motif autophosphorylation and induces the unprimed conformation) (Antal et al., 2014; Behn-Krappa and Newton, 1999), further reduced the FRET ratio (Figure 3C). The FRET ratio of PKCβII Neu PS was indistinguishable from that of kinase-dead PKC (K371R). We next

examined the ability of these mutants to adopt the active conformation upon agonist stimulation. PDBu treatment caused an increase in FRET ratio for WT PKCβII, reflecting the conformational rearrangement of the N and C termini (Figure 3D). PKCβII Scram PS underwent a more rapid conformational transition and the FRET change plateaued at a lower amplitude (Figure 3D). No conformational change was observed for kinase-inactive PKCβII Scram PS K371R, PKCβII Neu PS, or PKCβII K371R (Figure 3D). These data suggest that while PKCβII Scram PS is loosely autoinhibited and rapidly adopts the open/active conformation in the presence of agonist, PKCβII Neu PS resembles unprimed PKC and is incapable of transitioning to the active state.

Upon agonist stimulation, cPKC isozymes translocate to plasma membrane where their C2 domain recognizes PIP_2 and C1B domain binds DAG. However, PKC that has not been properly processed by phosphorylation exists in an open conformation with unmasked C1 domains, resulting in localization to DAG-rich Golgi membranes (Antal et al., 2014; Scott et al., 2013). PKCβII Kinameleon reporter proteins that were incapable of acquiring or retaining priming phosphorylations (Neu PS, K371R, Scram PS K371R) translocated primarily to intracellular compartments resembling Golgi membranes following PDBu stimulation (Figure 3E). In contrast, PKCβII that was fully (WT) or partially (Scram PS) phosphorylated/autoinhibited primarily distributed to the plasma membrane (Figure 3E). Co-localization analysis between PKC and membrane-targeted CFP confirmed that PKCβII Neu PS co-distributed with the Golgi marker and WT PKCβII co-distributed with the plasma membrane marker upon PDBu stimulation (Figure 3F). Thus, disruption of the pseudosubstrate unmasks the C1 domains to promote interaction with Golgi membranes. To assess exposure of the C1 domains in the pseudosubstrate mutants, we used FRET to monitor real-time translocation of YFP-tagged PKC to plasma membrane-targeted CFP in live cells (Figure 3G). In response to PDBu, PKCβII Scram PS and PKCβII Neu PS translocated to the plasma membrane with significantly faster kinetics than WT PKCβII (Figure 3H; $t_{1/2}$= 2.3 ± 0.1 min and 3.1 ± 0.2 min, respectively, versus 5.0 ± 0.2 min), but with slower kinetics than kinase-dead PKCβII K371R (Figure 3H; $t_{1/2}$= 1.0 ± 0.1 min), which has fully exposed C1 domains. The accelerated membrane translocation and enhanced affinity for Golgi membranes of the pseudosubstrate mutants support an unprimed, open conformation.

We next assessed the relationship between pseudosubstrate-dependent conformational changes and PKC activity using CKAR (Figure 3I). Addition of PKC inhibitor caused a minimal decrease in CKAR phosphorylation in cells expressing WT PKCβII, indicating low basal activity and effective autoinhibition, but a large decrease in cells expressing PKCβII Neu PS or PKCβII ΔPS, reflecting high basal activity and no autoinhibition. PKCβII Scram PS had slightly lower basal activity than that of the constitutively active PKCβII Neu PS, consistent with weak autoinhibition. Lastly, whereas WT PKCβII was phosphorylated at all three priming sites, the pseudosubstrate mutants had impaired phosphorylation: the weakly autoinhibited PKCβII Scram PS was minimally phosphorylated, while the unprimed PKCβII Neu PS and PKCβII ΔPS had no detectable phosphorylation (Figure 3J). Thus, the degree of PKC phosphorylation correlates with the extent of autoinhibition.

Autoinhibition Protects PKC from PHLPP1-Mediated Dephosphorylation and Degradation

We next investigated whether autoinhibition-deficient PKC was subject to dephosphorylation of the exposed hydrophobic motif site. We previously showed that activation of pure PKC via membrane binding increases its sensitivity to phosphatases by two orders of magnitude (Dutil et al., 1994). Furthermore, this phosphatase sensitivity is prevented by occupancy of the active site with protein or peptide substrates, or with small-molecule inhibitors (Cameron et al., 2009; Dutil and Newton, 2000; Gould et al., 2011). To assess whether the pseudosubstrate of PKC can similarly protect the kinase domain from dephosphorylation *in trans*, we examined the phosphorylation state of the isolated catalytic domain (Cat) expressed alone or co-expressed with the isolated regulatory domain containing (Reg) or lacking (Reg ΔPS) the pseudosubstrate (Figure 4A). The catalytic domain alone was not phosphorylated at either of the C-terminal priming sites in COS7 cells; however, co-expression with the PKC regulatory domain (Cat + Reg) was sufficient to rescue phosphorylation at the hydrophobic motif but not the turn motif (Figure 4B). Co-expression with the regulatory domain lacking the pseudosubstrate (Cat + Reg ΔPS), in contrast, did not promote catalytic domain hydrophobic motif phosphorylation (Figure 4B). These data reveal that autoinhibition by the pseudosubstrate is responsible for retaining phosphate specifically at the hydrophobic motif.

We next addressed whether the known hydrophobic motif phosphatase PHLPP was responsible for the dephosphorylation of newly-synthesized autoinhibition-deficient PKC. We employed pulse-chase analysis to ^{35}S radiolabel a pool of newly-synthesized PKC and monitored the maturation of the nascent protein via the electrophoretic mobility shift that accompanies phosphorylation (Borner et al., 1989; Sonnenburg et al., 2001). The kinetics of PKC phosphorylation were unaffected by ectopic PHLPP1 expression (Figure 4C), indicating that PHLPP1 may be saturating in any regulation of PKC. Immunoprecipitation revealed that PHLPP1 exclusively bound the faster mobility, unphosphorylated species of ^{35}S-labeled (newly-synthesized) PKC and did not bind the slower mobility band that became phosphorylated by 60 min (Figure 4C; asterisk). Further co-immunoprecipitation studies revealed that PHLPP1 effectively bound unphosphorylated ΔPS or kinase-dead (K371R) PKCβII mutants, independent of the C1A, C1B, or C2 domains as mutants lacking these regulatory domains still associated with PHLPP1 (Figure 4D). Deletion of the C2 domain with the pseudosubstrate intact (ΔC2) also resulted in enhanced PHLPP1 association (Figure 4D), consistent with our previous report that the C2 domain clamps the pseudosubstrate in the substrate-binding cavity (Antal et al., 2015a). Analysis of phosphorylation state and CKAR-reported activity revealed that the PKCβII ΔC2 mutant had decreased phosphorylation and enhanced basal activity, consistent with a loosening of autoinhibition as observed upon disruption of pseudosubstrate binding (Figure 4E, 4F). Deletion of the C1 and C2 domains concurrently (ΔC1A/C1B/C2) resulted in greater dephosphorylation than that observed upon deletion of the C2 domain alone (ΔC2). However, PKCβII ΔC1A/C1B/C2, which retains only the pseudosubstrate segment of the regulatory domain, was effectively autoinhibited: despite its enhanced sensitivity to dephosphorylation, its basal activity was indistinguishable from that of PKCβII ΔC1A, PKCβII ΔC2, and PKCβII ΔC1A/C1B, (Figure 4F). These data reveal that PHLPP1 interacts with a surface on the kinase domain of PKC that is masked by the regulatory domains upon autoinhibition, such that the

pseudosubstrate functions as a tether for the regulatory domain to occlude this interface and protect PKC from dephosphorylation.

We next used pulse-chase analysis to examine if phosphorylation could be detected on newly-synthesized autoinhibition-deficient PKC. PKCβII ΔPS, like kinase-dead PKC (K371R), did not undergo the characteristic mobility shift observed for WT PKC (Figure 4G). This finding suggests that PHLPP1 dephosphorylates newly-synthesized PKC that cannot be autoinhibited, thus preventing accumulation of the phosphorylated species on any "open" PKC.

Previous studies have shown that the isolated catalytic domain of PKC is phosphorylated at the priming sites when expressed in insect cells (Behn-Krappa and Newton, 1999), suggesting a different phosphatase environment in insect versus mammalian cells. To determine whether PKCβII ΔPS also evades dephosphorylation in this system, we analyzed the phosphorylation state of WT PKCβII or PKCβII ΔPS expressed in Sf9 cells. In marked contrast to its unphosphorylated state in mammalian cells, PKCβII ΔPS was phosphorylated at all three priming sites in Sf9 cells, revealing that PKC lacking the pseudosubstrate does incorporate phosphate but is dephosphorylated in the absence of autoinhibition in certain contexts, such as in COS7 cells (Figure 4H). Co-expression of the PP2C phosphatase domain of PHLPP1 caused a 4-fold decrease in both PKCβII WT and ΔPS steady-state levels, along with a commensurate decrease in phosphorylation, relative to cells that did not express the PHLPP1 PP2C domain (Figure 4H). The PHLPP1-induced decrease in steady-state levels and loss of the dephosphorylated species is consistent with the dephosphorylated protein displaying enhanced sensitivity to down-regulation (Figure 4H).

Upon dephosphorylation, PKC is subject to ubiquitination and proteasome-dependent degradation (Parker et al., 1995). Analysis of PKC's half-life via cycloheximide treatment of cells confirmed that autoinhibition-deficient PKC was significantly less stable than WT PKC (Figure 4I; WT PKCβII $t_{1/2}$ >48 hrs, Scram PS $t_{1/2}$=16 ± 2 hrs, Neu PS $t_{1/2}$=10.1 ± 0.5 hrs). Furthermore, endogenous PKCα was more resistant to PDBu- induced down-regulation in the absence of PHLPP1 (Figure 4J; *Phlpp1*$^{-/-}$ $t_{1/2}$= 14 ± 2 hrs, *Phlpp1*$^{+/+}$ $t_{1/2}$=6.6 ± 0.9 hrs). Moreover, the steady-state levels of endogenous PKCα were 2-fold higher in *Phlpp1*$^{-/-}$ MEFs compared to *Phlpp1*$^{+/+}$ MEFs (Figure 4K). These results demonstrate that unphosphorylated PKC is unstable and support a role for PHLPP1 in regulating PKC stability by opposing hydrophobic motif phosphorylation and consequently promoting PKC degradation.

Cancer-Associated Pseudosubstrate Hotspot Mutations Reveal a Distinct PKC LOF Mechanism

Given the tumor-suppressive role of PKCβ, we asked whether PKC mutations that perturb autoinhibition, and are thus subject to PHLPP1 quality control, could present a LOF mechanism in cancer. In support of this, the pseudosubstrate of PKCβ is a 3D-clustered functional hotspot of cancer-associated mutations (Gao et al., 2017). 10 distinct mutations, identified in 16 tumor samples, occur in the region preceding the P0 position (Ala^{25}) of the pseudosubstrate (P-7 through P-1) (Figure S3, Figure 5A). These include Arg^{22} at the P-3 position in the pseudosubstrate, a critical residue for effective autoinhibition which makes

multiple contacts with both the bound nucleotide and Asp^{470} in the active site (Figure 5B) (House and Kemp, 1990; Pears et al., 1990). Analysis of sequence conservation amongst PKC isozymes using the protein alignment tool KinView (McSkimming et al., 2016) reveals that this interaction partner, which resides between the HRD and DFG motifs of the kinase activation segment, is highly conserved in PKC isozymes compared to other kinases (Figure 5B; asterisk). Given the conservation of this interaction pair, we reasoned that the Arg^{22} mutations would have the largest effect on PKC autoinhibition. Introducing each of the 10 mutations into PKCβII, we measured basal activity via CKAR upon inhibitor addition in COS7 cells. The activity of every pseudosubstrate mutant differed significantly from that of WT and segregated into two distinct groups: 56% of mutations were less active than WT and 44% of mutations were more active (Figure 5C, 5D). Mutations displaying enhanced autoinhibition (Figure 5E; blue) had a higher fraction of phosphorylated PKC to unphosphorylated PKC compared to WT PKC, as assessed by the intensity of the slower-migrating phosphorylated species (asterisk) to the faster-migrating unphosphorylated species (dash) and staining with antibodies to the three processing phosphorylations (Figure 5E). Conversely, mutations displaying reduced autoinhibition (Figure 5E; red) had a lower fraction of phosphorylated PKC to unphosphorylated PKC compared to WT PKC (Figure 5E). Thus, mutants with reduced basal activity had increased phosphorylation relative to WT and mutants with increased basal activity had reduced phosphorylation (Figure 5F). These data show that aberrant autoinhibition of cancer-associated PKC pseudosubstrate mutations causes LOF in either of two ways: (1) enhancing pseudosubstrate affinity to reduce PKC output or (2) weakening pseudosubstrate affinity to reduce PKC phosphorylation and stability.

PKC Quality Control is Conserved in Human Cancer

More broadly, we explored whether PHLPP1-mediated quality control may be a ubiquitous mechanism employed by tumors to suppress PKC output. To assess whether PKC quality control by PHLPP1 is a conserved process in human cancer, we analyzed the phosphorylation state and total protein levels of PKC in patient tumor samples by reverse phase protein array (RPPA), a high-throughput antibody-based method for quantitative detection of protein markers from cell lysates (Tibes et al., 2006). Analysis of 5,157 patient samples from 19 cancers comprising The Cancer Genome Atlas (TCGA) Pan-Can 19 revealed a striking 1:1 correlation between PKCα hydrophobic motif phosphorylation ($pSer^{657}$) and total PKCα protein (Figure 6A, 6B; R=0.9301). We also analyzed hydrophobic motif phosphorylation of Akt and S6K, two other AGC kinases regulated by PHLPP1. In contrast to PKC, hydrophobic motif phosphorylation of Akt ($pSer^{473}$) and S6K ($pThr^{389}$) did not correlate with total protein (Figure 6A, 6B; R=0.1709 and 0.0939, respectively). Consistent with the tumor data, analysis of cancer cell lines from the Cancer Cell Line Encyclopedia (CCLE) and MD Anderson Cell Lines Project (MCLP) also displayed a strong correlation between PKCα hydrophobic motif phosphorylation ($pSer^{657}$) and total PKCα protein, which was not observed with the Akt activation loop ($pThr^{308}$) or hydrophobic motif ($pSer^{473}$) phosphorylation sites and total Akt protein (Figure S4). These data demonstrate that the hydrophobic motif site is generally phosphorylated in essentially 100% of the PKC species present in the cell, regardless of cell or tissue type. The one exception may be head and neck squamous carcinomas (HNSC), where a small number of

samples had hypophosphorylated PKC; whether defects in the PKC degradation pathway allow accumulation of unphosphorylated PKC in this cancer remains to be determined. In summary, RPPA analyses validate cellular studies showing that unphosphorylated PKC is unstable and rapidly degraded, indicating that only phosphorylated PKC accumulates in cells in an endogenous context.

High PKC and Low PHLPP1 Levels are Protective in Pancreatic Adenocarcinoma

We next sought to identify which cancer subtype exhibits the most robust PKC quality control by PHLPP1, a finding that could be therapeutically relevant. We reasoned that cancers in which PKC phosphorylation was strongly dependent on PHLPP1 would have (1) a strong correlation between PKCα and PKCβ hydrophobic motif phosphorylation due to common regulation of their levels and (2) have relatively low PKC steady-state levels because of dominant regulation by PHLPP1. Thus, we examined the correlation of total PKCα and PKCβ hydrophobic motif phosphorylation as a function of cancer type (Figure 7A; column 2). We also examined the association of known positive regulators of PKC processing, such as PDK-1 and mTORC2 components, with the PKCα:PKCβ hydrophobic motif correlation (Figure 7A; columns 3-7). In general, cancers with relatively high levels of PKC expression (e.g. low grade glioma (LGG), glioblastoma multiforme (GBM), and kidney renal papillary cell carcinoma (KIRP)) had relatively high correlation with these positive regulators, and those with low levels of PKC expression had low correlation with these positive regulators. One notable outlier was pancreatic adenocarcinoma (PAAD), which showed similar correlation signatures with positive regulators as those observed in high PKC-expressing cancers despite much lower PKCα expression levels (Figure 7A). Thus, we hypothesized that PKC expression in PAAD, which is suppressed by a common mechanism due to the strong correlation of PKCα:PKCβ hydrophobic motif phosphorylation (Figure 7A; column 2), may be dominantly regulated by PHLPP1 quality control. Indeed, RPPA analysis of the 105 PAAD samples revealed an inverse correlation between PHLPP1 levels and PKCα levels (Figure 7B and 7C). In contrast, this inverse correlation between PHLPP1 levels and PKCα was not observed in the glioma tumor samples (Figure 7B), two cancers in which positive regulators dominate in controlling PKC levels. This suggests that in gliomas, which generally have very low levels of PHLPP1 (Warfel et al., 2011), positive regulators dominate in controlling PKC levels (e.g. the positive regulators). However, in pancreatic cancer, PKC levels are determined by the negative regulator PHLPP1 via PKC quality control, as evidenced by the inverse correlation between PHLPP1 and PKCα protein levels. Together, these findings reveal a consistent 1:1 stoichiometry of PHLPP1 and PKC regardless of cell or tumor type; and in some cancers, such as pancreatic (but not glioblastoma), the amount of PHLPP1 is the dominant mechanism controlling the amount of PKC.

We next measured the impact of PKC levels on patient outcome by stratifying survival rates by levels of PKC hydrophobic motif phosphorylation. We focused on pancreatic cancer as PKC levels are subject to PHLPP1-mediated quality control in this cancer. Analysis of the cohort of 105 PAAD patients revealed that high levels of hydrophobic motif phosphorylation in PKCα (pSer^{657}) or PKCβ (pSer^{660}) co-segregated with significantly improved survival (Figure 7D). Thus, as PKC hydrophobic motif phosphorylation demarcates stable PKC and

improved patient survival, it serves as a potential prognostic marker and avenue for intervention in pancreatic cancer, for which there are limited effective therapeutic options.

DISCUSSION

The pseudosubstrate and phosphorylation play an interdependent and essential function in PKC homeostasis that is exploited in cancer to effectively lose PKC. First, phosphorylation of the hydrophobic motif is necessary for the pseudosubstrate-dependent transition of newly-synthesized PKC to the mature, autoinhibited conformation that prevents basal signaling in the absence of second messengers. In this manner, phosphorylation serves as an “off’ switch, ensuring that the deregulated activity of newly-synthesized enzyme is immediately quenched (Figure 7E; iii). This pseudosubstrate-engaged conformation, in turn, is necessary to protect newly-synthesized PKC from dephosphorylation by bound PHLPP1 (Figure 7E; ii). Because lack of phosphate at the hydrophobic motif results in proteasomal degradation of PKC, PHLPP1 provides a quality control step that prevents aberrant PKC from accumulating in the cell (Figure 7E; v). The vulnerability of aberrant PKC to dephosphorylation/degradation is exploited in cancer. Notably, the pseudosubstrate is a hotspot for cancer-associated mutations. Those that loosen autoinhibition are LOF because phosphorylation cannot be retained at the hydrophobic motif, resulting in an unstable protein that is degraded (Figure 7E, vi). Those that enhance autoinhibition are also LOF by decreasing signaling output, pushing the equilibrium to the closed conformation (Figure 7, iii). Validating the requirement for phosphorylation at the hydrophobic motif for PKC stability, analysis of over 5,000 tumor samples and 1,500 cell lines reveals an almost 1:1 correlation between total PKC levels and hydrophobic motif phosphorylation. Additionally, we identify PAAD as a malignancy in which PHLPP1 quality control dominates in controlling PKC levels. Consistent with a tumor-suppressive role of PKC, low levels of PKC are associated with poor survival outcome in this cancer. Thus, in PAAD, there is a dependence upon PHLPP1 to suppress PKC expression, providing a potential therapeutic target to stabilize PKC and increase patient survival.

Our findings delineate a mechanism that results in the loss of a tumor suppressor at the post-translational level, rather than the prevalent mechanism involving genetic deletion of regions encoding tumor suppressor genes (Weinberg, 1991). Indeed, the tumor-suppressive role of PKC isozymes remained uncharacterized for several decades, in part due to relatively infrequent deletion of PKC genes compared to other notable tumor suppressors. However, impairing protein stability is an equally effective method for LOF, as epitomized by the tumor suppressor p53, which is also stabilized by phosphorylation to prevent its degradation in the context of the DNA damage response (Chehab et al., 1999).

Attesting to its key regulatory role, the hydrophobic motif was recently identified as a hotspot for cancer mutations across most AGC kinases, including PKCβ (Huang et al., 2018). However, phosphate at this PHLPP-regulated position plays distinct roles among these kinases. For Akt and S6K, dephosphorylation at the hydrophobic motif attenuates catalytic activity (Gao et al., 2005; Liu et al., 2011) without affecting stability. This latter point is evident from our own analysis showing no significant correlation between the total levels of these two AGC kinases and phosphorylation of their respective hydrophobic motifs.

But in PKC, phosphorylation serves a very different function: it allows the pseudosubstrate to be tethered in the substrate-binding cavity to mediate autoinhibition and promote the stable conformation that results in a long half-life of PKC in cells. Thus, PKC is unique among PHLPP1 hydrophobic motif substrates in that phosphate protects the kinase from degradation.

An unexpected finding from this study is that deletion of the autoinhibitory pseudosubstrate abolished any detectable phosphorylation at the three processing sites yet resulted in constitutively and maximally active PKC. Thus, surprisingly, PKC with no priming phosphates can have full, unrestrained catalytic activity. Furthermore, as is the case for the activation loop phosphate (Sonnenburg et al., 2001), transient phosphorylation at the hydrophobic motif is necessary for PKC to progress to a catalytically-competent conformation, but then becomes dispensable for activity. We were unable to observe even transient phosphorylation of the autoinhibition-deficient PKC during processing in mammalian cells, underscoring the strict homeostatic control of the hydrophobic motif site. Phosphorylation of autoinhibition-deficient PKC, however, was readily observed in Sf9 insect cells. PKC may evade PHLPP quality control in insect cells because of the evolutionary functional divergence of the PHLPP PH domain (Park et al., 2008), a key determinant in its dephosphorylation of PKC in cells (Gao et al., 2008). One possible explanation for the requirement of negative charge at the hydrophobic motif early in the life cycle of PKC is that autophosphorylation of this site triggers association of the C-tail with the kinase domain, an important step in aligning the regulatory spine (Taylor and Kornev, 2011).

Although protein kinases share a common active conformation, numerous mechanisms of autoinhibition have evolved to maintain kinases in inactive states (Bayliss et al., 2015). For nearly all protein kinases, phosphorylation serves to relieve autoinhibition, usually elicited by binding to regulatory molecules following agonist stimulation. For example, Akt autoinhibition by the PH domain is relieved via binding phosphatidylinositol-3,4,5-trisphosphate (PIP_3) to promote activating phosphorylations at the activation loop and hydrophobic motif (Alessi et al., 1996). Indeed, oncogenic mutations that dislodge the PH domain from the kinase domain activate Akt independently of PIP_3 generation (Parikh et al., 2012). In a similar manner, we find that cancer-associated PKC mutations in the pseudosubstrate also elicit constitutive activity. However, by impairing autoinhibition, these mutations induce PHLPP1-dependent dephosphorylation and are effectively LOF by promoting PKC degradation. Thus, cancer-associated activating mutations that disrupt autoinhibition present as gain-of-function mutations in Akt but manifest as LOF mutations in PKC.

The role of PHLPP1 quality control in setting the level of PKC in cells has important ramifications for cancer therapies, as higher expression levels of PKC isozymes have been reported to predict improved patient survival in diverse malignancies (Newton, 2018). For example, higher levels of PKCα and PKCβII protein predict improved outcome in T-cell acute lymphoblastic leukemia (T-ALL) and colorectal cancer, respectively (Dowling et al., 2016; Milani et al., 2014). Here, we show that high PKC hydrophobic motif phosphorylation correlated with dramatically increased survival in PAAD. Because greater than 90% of

pancreatic cancers harbor an activating K-Ras mutation (Almoguera et al., 1988), one possibility is that high PKC levels suppress K-Ras signaling. Consistent with this, PKC phosphorylation of K-Ras on Ser^{181} in the farnesyl-electrostatic switch was reported to disengage K-Ras from the plasma membrane (Bivona et al., 2006). Although the role of this specific PKC phosphorylation in tumors is unclear (Barcelo et al., 2014), McCormick and colleagues have shown that oral administration of a phorbol ester with very weak potency promoted K-Ras phosphorylation and repressed growth in orthotopic mouse models of human pancreatic cancer (Wang et al., 2015). Furthermore, PKC suppresses growth of oncogenic K-Ras driven tumors in a xenograft mouse model of colorectal adenocarcinoma, and deletion or mutation of only one PKC allele is sufficient to enhance tumor growth (Antal et al., 2015b). Additionally, K-Ras is among the most frequently co-mutated genes in tumors with LOF PKC mutations (Antal et al., 2015b). Together, these data support a role for functional PKC in suppressing oncogenic K-Ras signaling. Another mechanism by which PKC suppresses oncogenic signaling was recently unveiled by Black and coworkers, who showed that PKCα deficiency in endometrial tumors enhances oncogenic Akt signaling via a mechanism involving its modulation of the activity of a PP2A family phosphatase (Hsu et al., 2018). Thus, targeting the PHLPP1-dependent quality control step of PKC processing may be a promising approach to stabilize PKC in cancers involving oncogenes controlled by PKC.

Our work underscores the importance of careful consideration of PKC phosphorylation mechanisms in cancer therapies. Notably, mTOR kinase inhibitors and Hsp90 inhibitors currently in clinical trials will have the unwanted result of preventing PKC processing, thus depleting levels of this tumor suppressor. Coupling such therapies with disruption of PHLPP1-dependent quality control may have significant therapeutic benefit. Thus, the post-translational inactivation of PKC by PHLPP1, distinct from loss of other tumor suppressors via genetic mechanisms, presents a druggable interaction and potential vulnerability in cancers that respond to PKC restoration.

STAR★METHODS

CONTACT FOR REAGENT AND RESOURCE SHARING

Further information and requests for resources and reagents should be directed to and will be fulfilled by the Lead Contact, Alexandra Newton (anewton@ucsd.edu).

EXPERIMENTAL MODEL AND SUBJECT DETAILS

Cell Culture and Transfection—COS7 cells, *Phlpp1*$^{+/+}$ MEFs, and *Phlpp1*$^{-/-}$ MEFs were cultured in DMEM (Corning) containing 10% fetal bovine serum (Atlanta Biologicals) and 1% penicillin/streptomycin (Gibco) at 37°C in 5% CO_2. Generation of the PHLPP1 MEFs was described previously (Masubuchi et al., 2010). Transient transfection was carried out using the Lipofectamine 3000 Transfection Reagent (Thermo Fisher Scientific). Sf9 cells were grown in Sf-900 II SFM media (Gibco) in shaking cultures at 27°C.

METHOD DETAILS

Plasmids and Constructs—The C Kinase Activity Reporter (CKAR) was previously described (Violin et al., 2003). PKC pseudosubstrate-deleted constructs were generated by looping out the 54 bases comprising residues 19-36 of PKCα or PKCβII by QuikChange Mutagenesis (Agilent). Scrambled and Neutral Pseudosubstrate constructs were generated by QuikChange Mutagenesis (Agilent). The catalytic domain was generated by cloning residues 296-673 of human PKCβII into pcDNA3 containing an N-terminal HA tag at the NotI and XbaI sites. Regulatory domain constructs were generated by cloning residues 1-295 of human PKCβ into pcDNA3 with mCherry at the N-terminus at the BamHI and XbaI sites. mCherry-tagged constructs were cloned into pcDNA3 with mCherry at the N-terminus at the BamHI and XbaI sites. mYFP-tagged constructs were cloned into pcDNA3 with mYFP at the N-terminus at the XhoI and XbaI sites. HA-tagged rat PKCβII constructs were cloned into pcDNA3 with HA at the N-terminus at the NotI and XbaI sites. HA-tagged human PKCβII constructs were cloned into pcDNA3 with HA at the N-terminus at the XhoI and XbaI sites. Kinameleon was cloned into pcDNA3 as mYFP-PKCβII-mCFP. All mutants were generated by QuikChange Mutagenesis (Agilent). Rat PKC constructs were used with the exception of human PKCα in Figure 2D and human PKCβII in Figures 5C, 5D, and 5E.

FRET Imaging and Analysis—Cells were imaged as described previously (Gallegos et al., 2006). For activity experiments COS7 cells were co-transfected with the indicated mCherry-tagged PKC construct and CKAR. For Kinameleon experiments, the indicated Kinameleon construct containing mYFP and mCFP was transfected alone. For translocation experiments, COS7 cells were co-transfected with the indicated mYFP-tagged construct and plasma-membrane targeted mCFP at a ratio of 10:1. Baseline images were acquired every 15 s for 2 min prior to ligand addition. Forster resonance energy transfer (FRET) ratios represent mean ± SEM from at least three independent experiments. All data were normalized to the baseline FRET ratio of each individual cell unless noted that absolute FRET ratio was plotted or traces were normalized to levels post-inhibitor addition. When comparing translocation kinetics, data were also normalized to the maximal amplitude of translocation for each, as previously described, in order to compare translocation rates (Antal et al., 2014). Every experiment contained an mCherry-transfected control to measure endogenous activity, and an mCherry-tagged WT (or deleted pseudosubstrate) PKC. Control traces are depicted as dotted lines: specifically, the endogenous trace in Figure 1E and the deleted pseudosubstrate trace in Figure 2G and 3I, were redrawn to serve as a point of reference in those Figures (data were acquired and derived in the same experiments which generated all the data in Figure 1 and Figure 2, respectively).

Immunoblotting and Antibodies—Cells were lysed in PPHB: 50 mM $NaPO_4$ (pH 7.5), 1% Triton X-100, 20 mM NaF, 1 mM $Na_4P_2O_7$, 100 mM NaCl, 2 mM EDTA, 2 mM EGTA, 1 mM Na_3VO_4, 1 mM PMSF, 40 mg/ml leupeptin, 1mM DTT, and 1 mM microcystin. *Phlpp1*$^{+/+}$ and *Phlpp1*$^{-/-}$ MEFs were lysed in 50 mM Tris (pH 7.4), 1% Triton X-100, 50 mM NaF, 10 mM Na4P2O7, 100 mM NaCl, 5 mM EDTA, 1 mM Na_3VO_4, 1 mM PMSF, 40 mg/ml leupeptin, and 1 mM microcystin. Triton-soluble fractions were analyzed by SDS-PAGE on 7% big gels to observe phosphorylation shift, transfer to PVDF membrane (Biorad), and western blotting via chemiluminescence SuperSignal West reagent (Thermo

Fisher) on a FluorChem Q imaging system (ProteinSimple). In Western blots, the asterisk (*) denotes the position of mature, phosphorylated PKC; whereas, the dash (−) indicates the position of unphosphorylated PKC. The turn motif and hydrophobic motif phosphorylations, but not the activation loop phosphorylation, induces an electrophoretic mobility shift that retards the migration of the phosphorylated species. The pan anti-phospho-PKC activation loop antibody (PKC pThr^{500}) was described previously (Dutil et al., 1998). The anti-phospho-PKCα/βII turn motif (pT638/641; 9375S) and pan anti-phospho-PKC hydrophobic motif (βII pS660; 9371S) antibodies and Calyculin A were purchased from Cell Signaling. Anti-PKCβ (610128) and PKCα (610128) antibodies were purchased from BD Transduction Laboratories. The DsRed antibody was purchased from Clontech. The anti-PHLPP1 antibody was purchased from Proteintech (22789-1-AP). The anti-HA antibody for immunoblot was purchased from Roche. The anti-HA (clone 16B12; 901515) and anti-FLAG (Clone L5; 637301) antibodies used for immunoprecipitation were purchased from BioLegend. The anti-α-tubulin (T6074) and anti-His (H1029) antibodies were from Sigma.

Baculovirus Expression of PKC and PHLPP1 PP2C—Human PKCβII, PKCβII ΔPS, and PHLPP1 PP2C (residues 1154-1422) were cloned into the pFastBac vector (Invitrogen) containing an N-terminal GST or His tag. Using the Bac-to-Bac Baculovirus Expression System (Invitrogen), the pFastBac plasmids were transformed into DH10Bac cells, and the resulting bacmid DNA was transfected into Sf9 insect cells via CellFECTIN (ThermoFisher Scientific). Sf9 cells were grown in Sf-900 II SFM media (Gibco) in shaking cultures at 27°C. The recombinant baculoviruses were harvested and amplified. Sf9 cells were seeded in 35 mm dishes (1×10^6 cells/dish) and infected with baculovirus. Following 2 days of incubation, Sf9 cells were lysed directly in 1x Laemmli sample buffer, sonicated, and boiled at 95°C for 5 min.

Pulse-Chase Experiments—For pulse-chase experiments, COS7 cells were incubated with Met/Cys-deficient DMEM for 30 min at 37 °C. The cells were then pulse-labeled with 0.5 mCi/ml [^{35}S]Met/Cys in Met/Cys-deficient DMEM for 7 min at 37 °C, media were removed, washed with dPBS (Corning), and chased with DMEM culture media (Corning) containing 200 mM unlabeled methionine and 200 mM unlabeled cysteine. At the indicated times, cells were lysed in PPHB and centrifuged at 13,000 x g for 3 min at 22 °C, supernatants were pre-cleared for 30 min at 4 °C with Protein A/G Beads (Santa Cruz), and protein complexes were immunoprecipitated from the supernatant with either an anti-HA or anti-FLAG monoclonal antibody (BioLegend, 16B12; BioLegend L5) overnight at 4 °C. The immune complexes were collected with Protein A/G Beads (Santa Cruz) for 2 hrs, washed 3x with PPHB, separated by SDS-PAGE, transferred to PVDF membrane (Biorad), and analyzed by autoradiography and western blot. Co-immunoprecipitation experiments were performed similarly, omitting the labeling and autoradiography steps.

Reverse Phase Protein Array—For RPPA experiments, patient samples and cell line samples were prepared and antibodies were validated as described previously (Li et al., 2017; Tibes et al., 2006).

Cancer Mutation Identification—Cancer-associated pseudosubstrate mutations were identified by querying the cBioPortal (cbioportal.org), COSMIC (https://cancer.sanger.ac.uk/cosmic), mutation3D (mutation3d.org), and ICGC (https://dcc.icgc.org) databases.

QUANTIFICATION AND STATISTICAL ANALYSIS

Statistical significance was determined via Repeated Measures One-Way ANOVA and Brown-Forsythe Test or Student's t-test performed in GraphPad Prism 6.0a (GraphPad Software). The half-time of translocation or degradation was calculated by fitting the data to a non-linear regression using a one-phase exponential association equation with GraphPad Prism 6.0a (GraphPad Software). Western blots were quantified by densitometry using the AlphaView software (Protein Simple).

Supplementary Material

Refer to Web version on PubMed Central for supplementary material.

ACKNOWLEDGMENTS

We thank Jon Violin for initial studies on PKC Scram/Neu PS. This work was supported by NIH R35 GM122523 and NIH GM43154 to ACN. TRB was supported by the PhRMA Foundation Pre Doctoral Fellowship in Pharmacology Toxicology (#20183844). TRB and ANV were supported by the UCSD Graduate Training Program in Cellular and Molecular Pharmacology (T32 GM007752).

REFERENCES

Alessi DR, Andjelkovic M, Caudwell B, Cron P, Morrice N, Cohen P, and Hemmings BA (1996). Mechanism of activation of protein kinase B by insulin and IGF-1. Embo J.Embo J 15, 6541–6551. [PubMed: 8978681]

Almoguera C, Shibata D, Forrester K, Martin J, Arnheim N, and Perucho M (1988). Most human carcinomas of the exocrine pancreas contain mutant c-K-ras genes. Cell 53, 549–554. [PubMed: 2453289]

Antal CE, Callender JA, Kornev AP, Taylor SS, and Newton AC (2015a). Intramolecular C2 Domain-Mediated Autoinhibition of Protein Kinase C βII. CellReports 12, 1252–1260.

Antal CE, Hudson AM, Kang E, Zanca C, Wirth C, Stephenson NL, Trotter EW, Gallegos LL, Miller CJ, Furnari FB, et al. (2015b). Cancer-associated protein kinase C mutations reveal kinase's role as tumor suppressor. Cell 160, 489–502. [PubMed: 25619690]

Antal CE, Violin JD, Kunkel MT, Skovso S, and Newton AC (2014). Intramolecular conformational changes optimize protein kinase C signaling. Chem Biol 21, 459–469. [PubMed: 24631122]

Balendran A, Hare GR, Kieloch A, Williams MR, and Alessi DR (2000). Further evidence that 3-phosphoinositide-dependent protein kinase-1 (PDK1) is required for the stability and phosphorylation of protein kinase C (PKC) isoforms. FEBS letters 484, 217–223. [PubMed: 11078882]

Barcelo C, Paco N, Morell M, Alvarez-Moya B, Bota-Rabassedas N, Jaumot M, Vilardell F, Capella G, and Agell N (2014). Phosphorylation at Ser-181 of oncogenic KRAS is required for tumor growth. Cancer research 74, 1190–1199. [PubMed: 24371225]

Bayliss R, Haq T, and Yeoh S (2015). The Ys and wherefores of protein kinase autoinhibition ☆. BBA -Proteins and Proteomics 1854, 1586–1594. [PubMed: 25936518]

Behn-Krappa A, and Newton AC (1999). The hydrophobic phosphorylation motif of conventional protein kinase C is regulated by autophosphorylation. Current biology : CB 9, 728–737. [PubMed: 10421574]

Bivona TG, Quatela SE, Bodemann BO, Ahearn IM, Soskis MJ, Mor A, Miura J, Wiener HH, Wright L, Saba SG, et al. (2006). PKC regulates a farnesyl-electrostatic switch on K-Ras that promotes its

association with Bcl-XL on mitochondria and induces apoptosis. Mol Cell 21, 481–493. [PubMed: 16483930]

Bornancin F, and Parker PJ (1997). Phosphorylation of protein kinase C-alpha on serine 657 controls the accumulation of active enzyme and contributes to its phosphatase- resistant state [published erratum appears in J Biol Chem 1997 May 16;272(20):13458]. The Journal of biological chemistry 272, 3544–3549. [PubMed: 9013603]

Borner C, Filipuzzi I, Wartmann M, Eppenberger U, and Fabbro D (1989). Biosynthesis and posttranslational modifications of protein kinase C in human breast cancer cells. The Journal of biological chemistry 264, 13902–13909. [PubMed: 2474538]

Brognard J, and Hunter T (2011). Protein kinase signaling networks in cancer. Curr Opin Genet Dev 21, 4–11. [PubMed: 21123047]

Callender JA, Yang Y, Lorden G, Stephenson NL, Jones AC, Brognard J, and Newton AC (2018). Protein kinase Calpha gain-of-function variant in Alzheimer's disease displays enhanced catalysis by a mechanism that evades down-regulation. Proceedings of the National Academy of Sciences of the United States of America 115, E5497–E5505. [PubMed: 29844158]

Cameron AJ, Escribano C, Saurin AT, Kostelecky B, and Parker PJ (2009). PKC maturation is promoted by nucleotide pocket occupation independently of intrinsic kinase activity. Nature structural & molecular biology.

Cazaubon S, Bornancin F, and Parker PJ (1994). Threonine-497 is a critical site for permissive activation of protein kinase C alpha. The Biochemical journal 301, 443–448.

Chehab NH, Malikzay A, Stavridi ES, and Halazonetis TD (1999). Phosphorylation of Ser-20 mediates stabilization of human p53 in response to DNA damage. Proc Natl Acad Sci U S A 96, 13777–13782. [PubMed: 10570149]

Dowling CM, Phelan J, Callender JA, Cathcart MC, Mehigan B, McCormick P, Dalton T, Coffey JC, Newton AC, O'Sullivan J, et al. (2016). Protein kinase C beta II suppresses colorectal cancer by regulating IGF-1 mediated cell survival. Oncotarget 7, 20919–20933. [PubMed: 26989024]

Dutil EM, Keranen LM, DePaoli-Roach AA, and Newton AC (1994). In vivo regulation of protein kinase C by trans-phosphorylation followed by autophosphorylation. The Journal of biological chemistry 269, 29359–29362. [PubMed: 7961910]

Dutil EM, and Newton AC (2000). Dual role of pseudosubstrate in the coordinated regulation of protein kinase C by phosphorylation and diacylglycerol. The Journal of biological chemistry 275, 10697–10701. [PubMed: 10744767]

Dutil EM, Toker A, and Newton AC (1998). Regulation of conventional protein kinase C isozymes by phosphoinositide-dependent kinase 1 (PDK-1). Current biology : CB 8, 1366–1375. [PubMed: 9889098]

Edwards AS, and Newton AC (1997). Phosphorylation at conserved carboxyl-terminal hydrophobic motif regulates the catalytic and regulatory domains of protein kinase C. The Journal of biological chemistry 272, 18382–18390. [PubMed: 9218480]

Gao J, Chang MT, Johnsen HC, Gao SP, Sylvester BE, Sumer SO, Zhang H, Solit DB, Taylor BS, Schultz N, et al. (2017). 3D clusters of somatic mutations in cancer reveal numerous rare mutations as functional targets. Genome Med 9, 4. [PubMed: 28115009]

Gao T, Brognard J, and Newton AC (2008). The Phosphatase PHLPP Controls the Cellular Levels of Protein Kinase C. Journal of Biological Chemistry 283, 6300–6311. [PubMed: 18162466]

Gao T, Furnari F, and Newton AC (2005). PHLPP: a phosphatase that directly dephosphorylates Akt, promotes apoptosis, and suppresses tumor growth. Molecular cell 18, 13–24. [PubMed: 15808505]

Gould CM, Antal CE, Reyes G, Kunkel MT, Adams RA, Ziyar A, Riveros T, and Newton AC (2011). Active site inhibitors protect protein kinase C from dephosphorylation and stabilize its mature form. The Journal of biological chemistry 286, 28922–28930. [PubMed: 21715334]

Griner EM, and Kazanietz MG (2007). Protein kinase C and other diacylglycerol effectors in cancer. Nat Rev Cancer 7, 281–294. [PubMed: 17384583]

Guertin DA, Stevens DM, Thoreen CC, Burds AA, Kalaany NY, Moffat J, Brown M, Fitzgerald KJ, and Sabatini DM (2006). Ablation in mice of the mTORC components raptor, rictor, or mLST8 reveals that mTORC2 is required for signaling to Akt-FOXO and PKCalpha, but not S6K1. Dev Cell 11, 859–871. [PubMed: 17141160]

Hansra G, Garcia-Paramio P, Prevostel C, Whelan RD, Bornancin F, and Parker PJ (1999). Multisite dephosphorylation and desensitization of conventional protein kinase C isotypes. Biochem J 342 (Pt 2), 337–344. [PubMed: 10455020]

House C, and Kemp BE (1987). Protein kinase C contains a pseudosubstrate prototope in its regulatory domain. Science 238, 1726–1728. [PubMed: 3686012]

House C, and Kemp BE (1990). Protein kinase C pseudosubstrate prototope: structure-function relationships. Cell Signal 2, 187–190. [PubMed: 2400634]

Hsu AH, Lum MA, Shim K-S, Frederick PJ, Morrison CD, Chen B, Lele SM, Sheinin YM, Daikoku T, and Dey SK (2018). Crosstalk between PKCα and PI3K/AKT Signaling Is Tumor Suppressive in the Endometrium. Cell reports 24, 655–669. [PubMed: 30021163]

Huang LC, Ross KE, Baffi TR, Drabkin H, Kochut KJ, Ruan Z, D'Eustachio P, McSkimming D, Arighi C, Chen C, et al. (2018). Integrative annotation and knowledge discovery of kinase post-translational modifications and cancer-associated mutations through federated protein ontologies and resources. Sci Rep 8, 6518. [PubMed: 29695735]

Jaken S, Tashjian AH Jr., and Blumberg PM (1981). Characterization of phorbol ester receptors and their down-modulation in GH4C1 rat pituitary cells. Cancer research 41, 2175–2181. [PubMed: 6786733]

Keranen LM, Dutil EM, and Newton AC (1995). Protein kinase C is regulated in vivo by three functionally distinct phosphorylations. Current Biology 5, 1394–1403. [PubMed: 8749392]

Le Good JA, Ziegler WH, Parekh DB, Alessi DR, Cohen P, and Parker PJ (1998). Protein kinase C isotypes controlled by phosphoinositide 3-kinase through the protein kinase PDK1. Science 281, 2042–2045. [PubMed: 9748166]

Li J, Zhao W, Akbani R, Liu W, Ju Z, Ling S, Vellano CP, Roebuck P, Yu Q, Eterovic AK, et al. (2017). Characterization of Human Cancer Cell Lines by Reverse-phase Protein Arrays. Cancer Cell 31, 225–239. [PubMed: 28196595]

Liu J, Stevens PD, Li X, Schmidt MD, and Gao T (2011). PHLPP-mediated dephosphorylation of S6K1 inhibits protein translation and cell growth. Molecular and cellular biology.

Lu Z, Liu D, Hornia A, Devonish W, Pagano M, and Foster DA (1998). Activation of protein kinase C triggers its ubiquitination and degradation. Molecular and cellular biology 18, 839–845. [PubMed: 9447980]

Masubuchi S, Gao T, O'Neill A, Eckel-Mahan K, Newton AC, and Sassone-Corsi P (2010). Protein phosphatase PHLPP1 controls the light-induced resetting of the circadian clock. Proceedings of the National Academy of Sciences 107, 1642–1647.

McSkimming DI, Dastgheib S, Baffi TR, Byrne DP, Ferries S, Scott ST, Newton AC, Eyers CE, Kochut KJ, Eyers PA, et al. (2016). KinView: a visual comparative sequence analysis tool for integrated kinome research. Molecular BioSystems 12, 3651–3665. [PubMed: 27731453]

Milani G, Rebora P, Accordi B, Galla L, Bresolin S, Cazzaniga G, Buldini B, Mura R, Ladogana S, Giraldi E, et al. (2014). Low PKCalpha expression within the MRD-HR stratum defines a new subgroup of childhood T-ALL with very poor outcome. Oncotarget 5, 5234–5245. [PubMed: 25026300]

Newton AC (2018). Protein kinase C: perfectly balanced. Crit Rev Biochem Mol Biol 53, 208–230. [PubMed: 29513138]

Orr JW, Keranen LM, and Newton AC (1992). Reversible exposure of the pseudosubstrate domain of protein kinase C by phosphatidylserine and diacylglycerol. The Journal of biological chemistry 267, 15263–15266. [PubMed: 1639770]

Orr JW, and Newton AC (1994). Requirement for Negative Charge on "Activation Loop" of Protein Kinase C. J. Biol. Chem. 269, 27715–27718. [PubMed: 7961692]

Parikh C, Janakiraman V, Wu WI, Foo CK, Kljavin NM, Chaudhuri S, Stawiski E, Lee B, Lin J, Li H, et al. (2012). Disruption of PH-kinase domain interactions leads to oncogenic activation of AKT in human cancers. Proc Natl Acad Sci U S A 109, 19368–19373. [PubMed: 23134728]

Park WS, Heo WD, Whalen JH, O'Rourke NA, Bryan HM, Meyer T, and Teruel MN (2008). Comprehensive identification of PIP3-regulated PH domains from C. elegans to H. sapiens by model prediction and live imaging. Mol Cell 30, 381–392. [PubMed: 18471983]

Parker PJ, Bosca L, Dekker L, Goode NT, Hajibagheri N, and Hansra G (1995). Protein kinase C (PKC)-induced PKC degradation: a model for down-regulation. Biochemical Society transactions 23, 153–155. [PubMed: 7758717]

Pears CJ, Kour G, House C, Kemp BE, and Parker PJ (1990). Mutagenesis of the pseudosubstrate site of protein kinase C leads to activation. European journal of biochemistry 194, 89–94. [PubMed: 2253627]

Scott AM, Antal CE, and Newton AC (2013). Electrostatic and hydrophobic interactions differentially tune membrane binding kinetics of the C2 domain of protein kinase Calpha. J Biol Chem 288, 16905–16915. [PubMed: 23589289]

Sonnenburg ED, Gao T, and Newton AC (2001). The phosphoinositide-dependent kinase, PDK-1, phosphorylates conventional protein kinase C isozymes by a mechanism that is independent of phosphoinositide 3-kinase. The Journal of biological chemistry 276, 45289–45297. [PubMed: 11579098]

Taylor SS, and Kornev AP (2011). Protein kinases: evolution of dynamic regulatory proteins. Trends Biochem Sci 36, 65–77. [PubMed: 20971646]

Tibes R, Qiu Y, Lu Y, Hennessy B, Andreeff M, Mills GB, and Kornblau SM (2006). Reverse phase protein array: validation of a novel proteomic technology and utility for analysis of primary leukemia specimens and hematopoietic stem cells. Mol Cancer Ther 5, 2512–2521. [PubMed: 17041095]

Violin JD, Zhang J, Tsien RY, and Newton AC (2003). A genetically encoded fluorescent reporter reveals oscillatory phosphorylation by protein kinase C. The Journal of cell biology 161, 899–909. [PubMed: 12782683]

Wang MT, Holderfield M, Galeas J, Delrosario R, To MD, Balmain A, and McCormick F (2015). K-Ras Promotes Tumorigenicity through Suppression of Non-canonical Wnt Signaling. Cell 163, 1237–1251. [PubMed: 26590425]

Warfel NA, Niederst M, Stevens MW, Brennan PM, Frame MC, and Newton AC (2011). Mislocalization of the E3 ligase, beta-transducin repeat-containing protein 1 (beta-TrCP1), in glioblastoma uncouples negative feedback between the pleckstrin homology domain leucine-rich repeat protein phosphatase 1 (PHLPP1) and Akt. J Biol Chem 286, 19777–19788. [PubMed: 21454620]

Weinberg RA (1991). Tumor suppressor genes. Science 254, 1138–1146. [PubMed: 1659741]

Zhang LL, Cao FF, Wang Y, Meng FL, Zhang Y, Zhong DS, and Zhou QH (2015). The protein kinase C (PKC) inhibitors combined with chemotherapy in the treatment of advanced non-small cell lung cancer: meta-analysis of randomized controlled trials. Clinical & translational oncology : official publication of the Federation of Spanish Oncology Societies and of the National Cancer Institute of Mexico 17, 371–377.

Highlights

- Phosphorylation of newly-synthesized PKC is necessary for stabilizing autoinhibition
- PHLPP1 dephosphorylates newly-synthesized PKC to provide quality control
- PKC quality control is conserved in >5,000 patient samples from 19 cancers
- Pancreatic cancer patients with high PKC and low PHLPP1 have improved survival

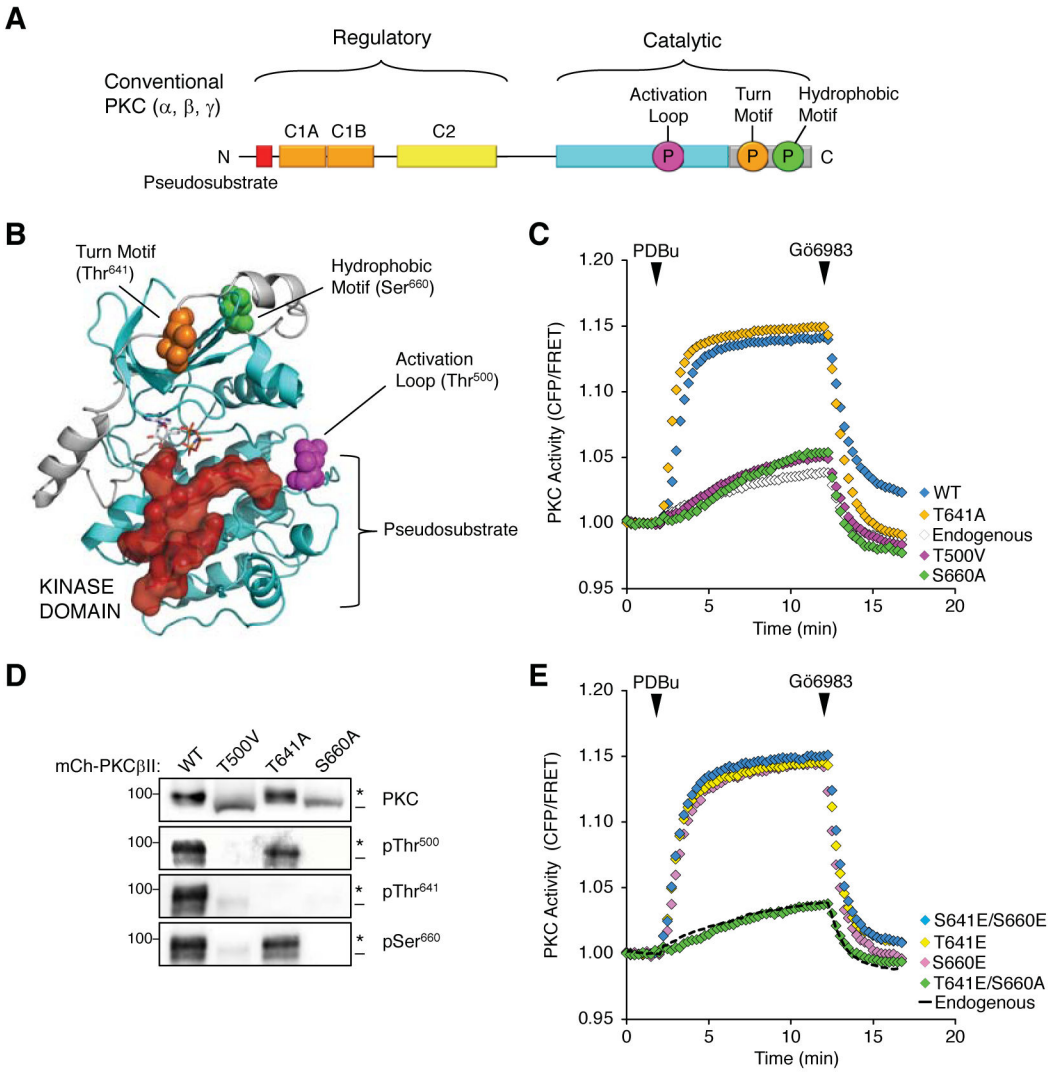

Figure 1. PKC Priming Phosphorylations are Necessary for Maturation and Activity

(**A**) cPKC domain structure showing pseudosubstrate (red), C1 domains (orange), C2 domain (yellow), kinase domain (cyan), C-terminal tail (grey), and three priming phosphorylations (circles).

(**B**) Crystal structure of PKCβII kinase domain (cyan; PDB ID 3PFQ) highlighting priming phosphorylations (space-filling) and pseudosubstrate residues 18-26 (red) modeled into the active site.

(**C**) COS7 cells expressing CKAR alone (Endogenous) or co-expressing the indicated mCherry-PKCβII WT or Ala mutant constructs were treated with PDBu (200nM) followed by Gö6983 (1μM).

(**D**) IB analysis of COS7 cells transfected with the indicated PKCβII constructs and probed with indicated phospho-specific or total PKC antibodies.

(**E**) COS7 cells expressing CKAR alone (Endogenous) or co-expressing the indicated mCherry-PKCβII phosphomimetic Glu substitution constructs were treated with PDBu (200nM) followed by Gö6983 (1μM).

CKAR data represent the normalized FRET ratio changes (mean ± SEM) from at least 3 independent experiments of >100 cells for each condition.

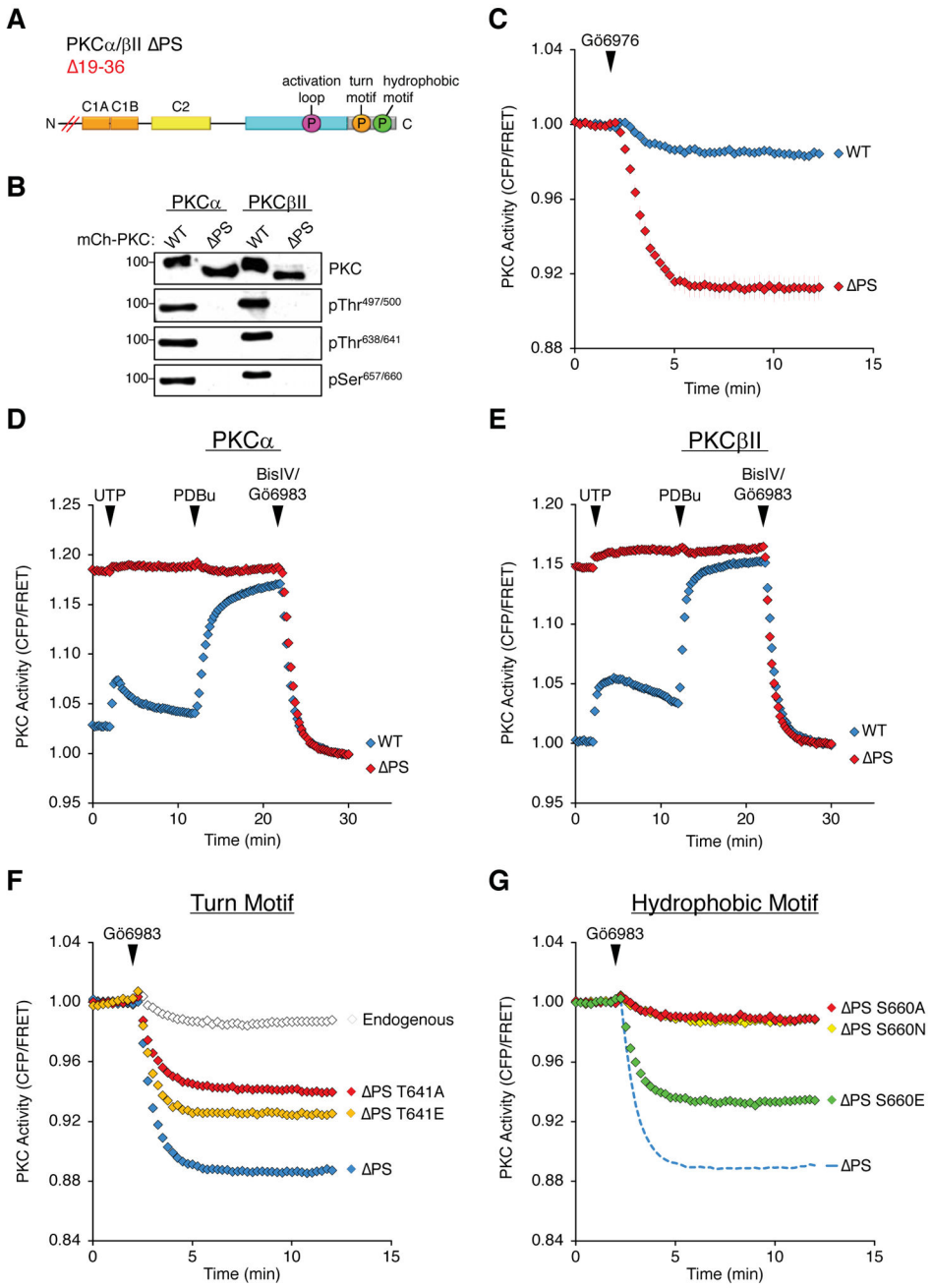

Figure 2. The Autoinhibitory Pseudosubstrate is Required for Cellular PKC Phosphorylation

(**A**) Schematic of pseudosubstrate-deleted PKC (ΔPS), lacking amino acids 19-36 of PKCα or PKCβII.

(**B**) IB analysis of lysates from COS7 cells transfected with indicated PKC constructs and probed with phospho-specific or total PKC antibodies.

(**C-G**) PKC activity analysis in COS7 cells expressing CKAR alone (Endogenous) or co-expressing the indicated mCherry-PKC constructs sequentially treated with agonists UTP (100μM), PDBu (200nM), and then inhibitors (BisIV (2μM) and Gö6983 (1μM), or Gö6976 (1μM)). PKCβII ΔPS trace in (F) is reproduced in (G) for comparison (dashed line).

CKAR data represent the normalized FRET ratio changes (mean ± SEM) from three independent experiments of >100 cells for each condition.

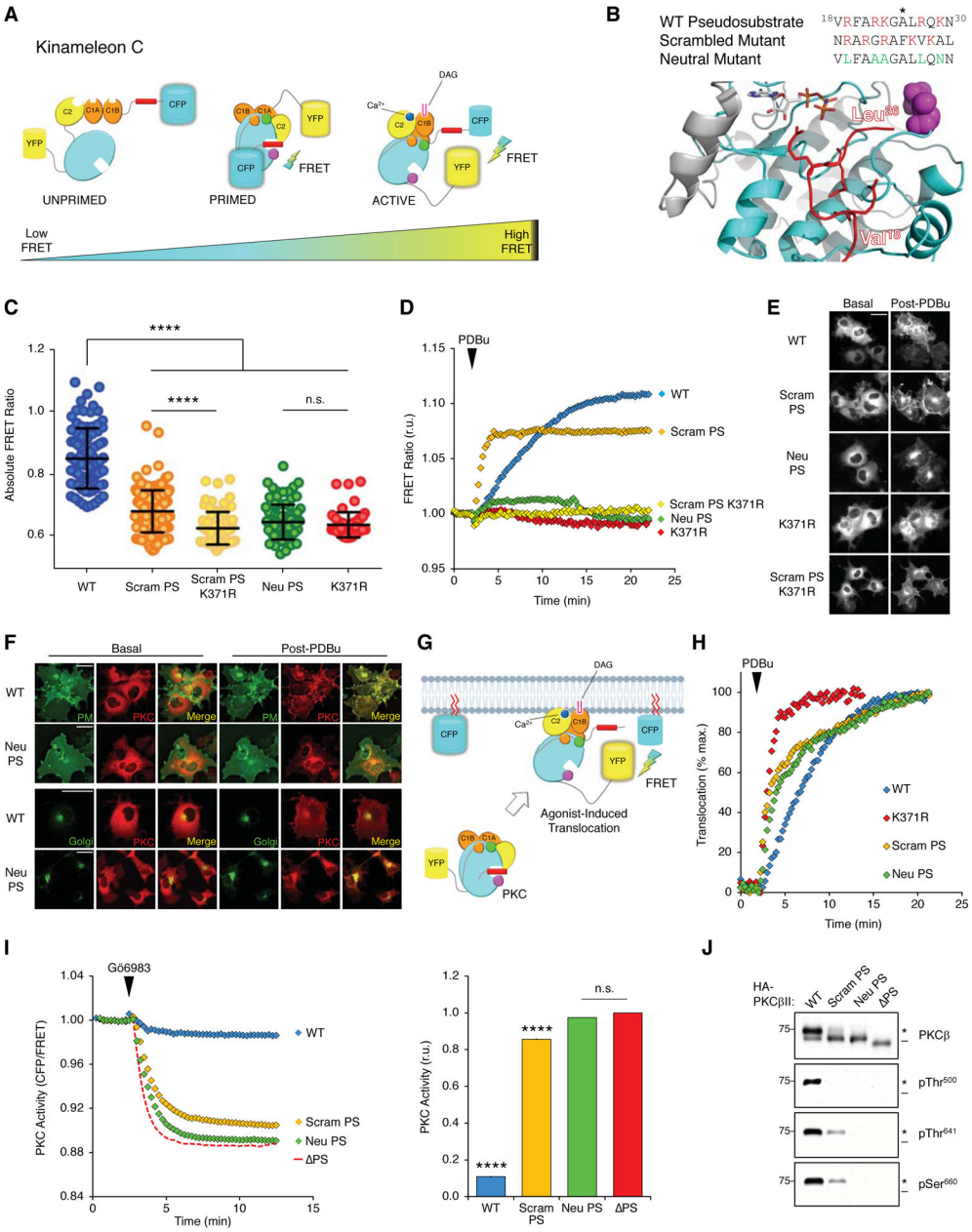

Figure 3. The Autoinhibited Conformation of PKC Retains Priming Phosphorylations

(**A**) Schematic showing PKC conformations assessed using the Kinameleon C FRET Reporter.

(**B**) PKCβII pseudosubstrate mutants with basic (red) and neutral residues (green) highlighted. Crystal structure of PKCβII showing the pseudosubstrate modeled into the active site of the kinase domain with basic residues shown as sticks. The pseudo-P-site is indicated by an asterisk (*).

(**C**) Absolute FRET ratio (mean ± SEM) of the indicated PKCβII Kinameleon C constructs expressed in COS7 cells. Each data point represents the average absolute FRET ratio from an individual cell.

(**D**) FRET ratio changes (mean ± SEM) of the indicated PKCβII Kinameleon C constructs expressed in COS7 cells following PDBu (200nM) treatment.
(**E**) Representative YFP images of indicated PKCβII Kinameleon C constructs in COS7 cells before (Basal) or after (Post-PDBu) 25 min stimulation with PDBu (200nM).
(**F**) Representative pseudo-colored images of plasma membrane-targeted (PM) or Golgi-targeted (Golgi) mCFP and the indicated mCherry-PKCβII in COS7 cells. Co-localization is shown as yellow in an overlay of mCFP and mCherry images (Merge).
(**G**) Schematic for PKC Translocation Assay: agonist-stimulated movement of mYFP-tagged PKC to plasma membrane-localized myristoylated-palmitoylated mCFP is monitored by FRET increase upon PKC membrane association.
(**H**) Translocation analysis of the indicated mYFP-PKCβII was monitored by FRET ratio change in COS7 cells co-expressing myristoylated-palmitoylated mCFP and treated with PDBu (100nM).
(**I**) Basal PKC activity in COS7 cells expressing CKAR and the indicated mCherry-PKCβII constructs treated with Gö6983 (1μM). Quantification (right) shows the normalized magnitude of FRET ratio change.
(**J**) IB analysis of lysates of COS7 cells expressing indicated PKCβII constructs and probed with indicated phospho-specific or total PKC antibodies.
****$p < 0.0001$, by Repeated Measures One-Way ANOVA and Brown-Forsythe Test; n.s., not significant. Kinameleon and CKAR represent the normalized FRET ratio changes (mean ± SEM) from three independent experiments with >100 cells for each condition.

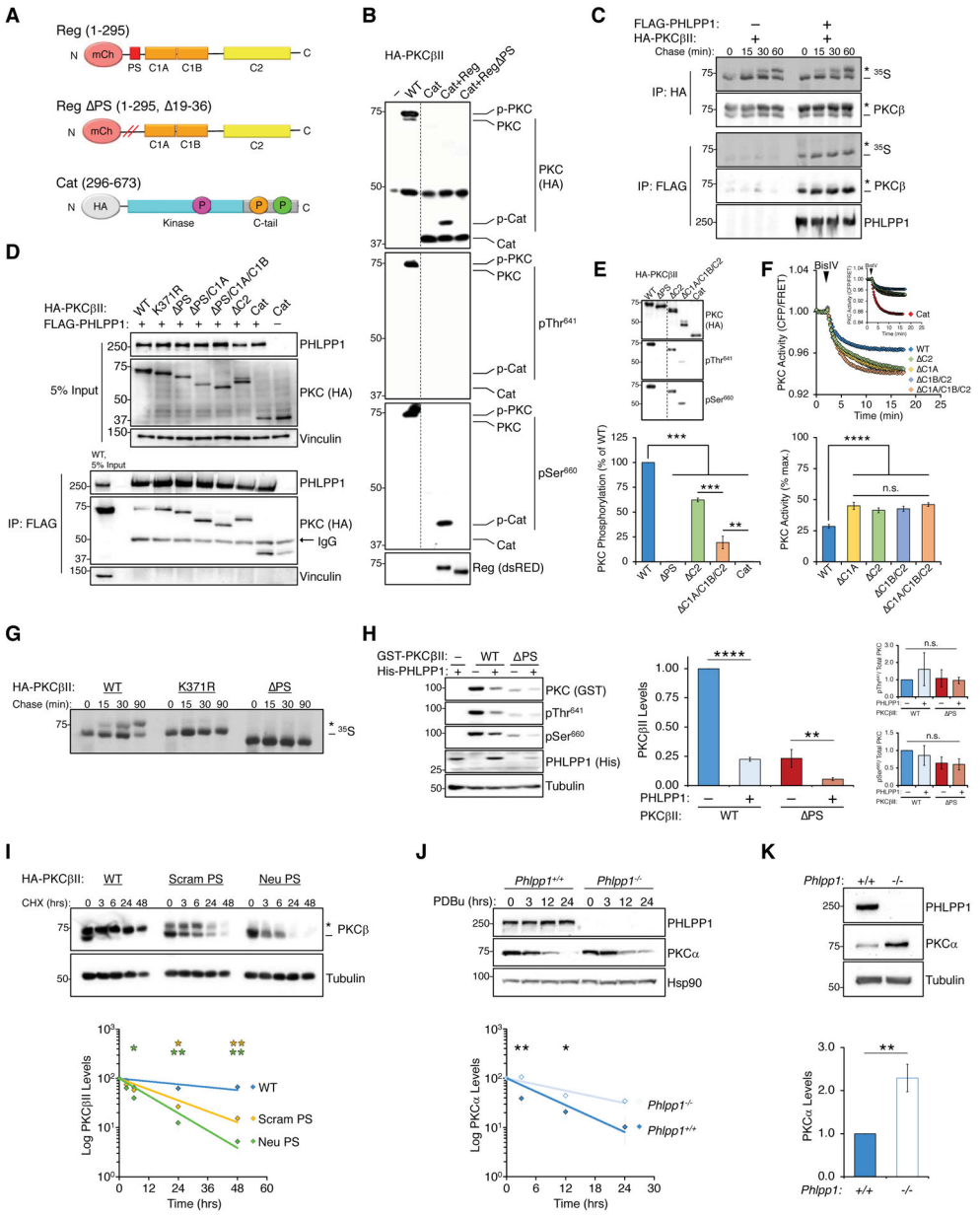

Figure 4. Autoinhibition Protects PKC from PHLPP1-Mediated Dephosphorylation and Degradation

(**A**) Schematic of indicated PKCβII truncation mutants.

(**B**) IB analysis of COS7 cells expressing indicated PKCβII constructs probed with indicated phospho-specific or total PKC antibodies.

(**C**) Autoradiogram (^{35}S) and IB analysis of newly-synthesized PKC pulse-chase immunoprecipitates from COS7 cells expressing HA-PKCβII and FLAG-PHLPP1 (see Methods).

(**D**) IB analysis of FLAG immunoprecipitates from COS7 cells transfected with indicated HA-PKCβII and FLAG-PHLPP1 constructs and probed with indicated antibodies. Vinculin was used as a loading control.

(**E**) IB analysis of lysates from COS7 cells transfected with indicated HA-PKCβII constructs probed with phospho-specific or total PKC antibodies. PKCβII Δ37-86 (ΔC1A), PKCβII Δ159-291 (ΔC2), PKCβII Δ101-291 (ΔC1B/C2), PKCβII Δ37-291 (ΔC1A/C1B/C2), or PKCβII 296-673 (Cat). Quantification (bottom) of $pSer^{660}$band intensity relative to WT (mean ± range, n=2).

(**F**) COS7 cells co-expressing CKAR and indicated mCherry-PKCβII regulatory domain deletion constructs were treated with BisIV (2μM). Insert shows trace for Cat activity, with cluster of traces in main figure reproduced for comparison. Quantification (bottom) shows magnitude of the FRET ratio change from 3 independent experiments.

(**G**) Autoradiogram (^{35}S) of HA immunoprecipitates from pulse-chase of COS7 cells expressing the indicated PKC constructs.

(**H**) IB analysis of lysates from Sf9 insect cells infected with the indicated GST-PKC constructs and His-Phlpp1 PP2C (PHLPP1; 1154-1422) baculovirus, probed with the indicated phospho-specific or total PKC antibodies. Quantification (right) of total PKC protein normalized to Tubulin or PKC phosphorylation normalized to total PKC.

(**I**) IB analysis of lysates from COS7 cells expressing the indicated HA-PKC constructs treated with cycloheximide (CHX, 250μM) for the indicated times prior to lysis and probed with the indicated antibodies. Quantification (bottom) of PKC band intensity normalized to Tubulin loading control and plotted as percentage of protein at time zero.

(**J**) IB analysis of lysates from WT (*Phlpp1*$^{+/+}$) or PHLPP1 knock-out (*Phlpp1*$^{-/-}$) MEFs treated with PDBu (200 nM) for the indicated time points prior to lysis and probed with the indicated antibodies. Quantification (bottom) of PKC band intensity normalized to Hsp90 loading control and plotted as percentage of protein at time zero.

(**K**) IB analysis of lysates from untreated WT (*Phlpp1*$^{+/+}$) or PHLPP1 knock-out (*Phlpp1*$^{-/-}$) MEFs probed with the indicated antibodies. Quantification (bottom) of PKC band intensity normalized to Tubulin loading control.

*p < 0.05, **p < 0.01, ***p < 0.001, ****p < 0.0001 by Repeated Measures One-Way ANOVA and Tukey HSD Test. IB quantification (excluding (E)) represent the mean ± SEM from at least three independent experiments. Dashed line ((B) and (E)) indicates splicing of irrelevant lanes from a single blot.

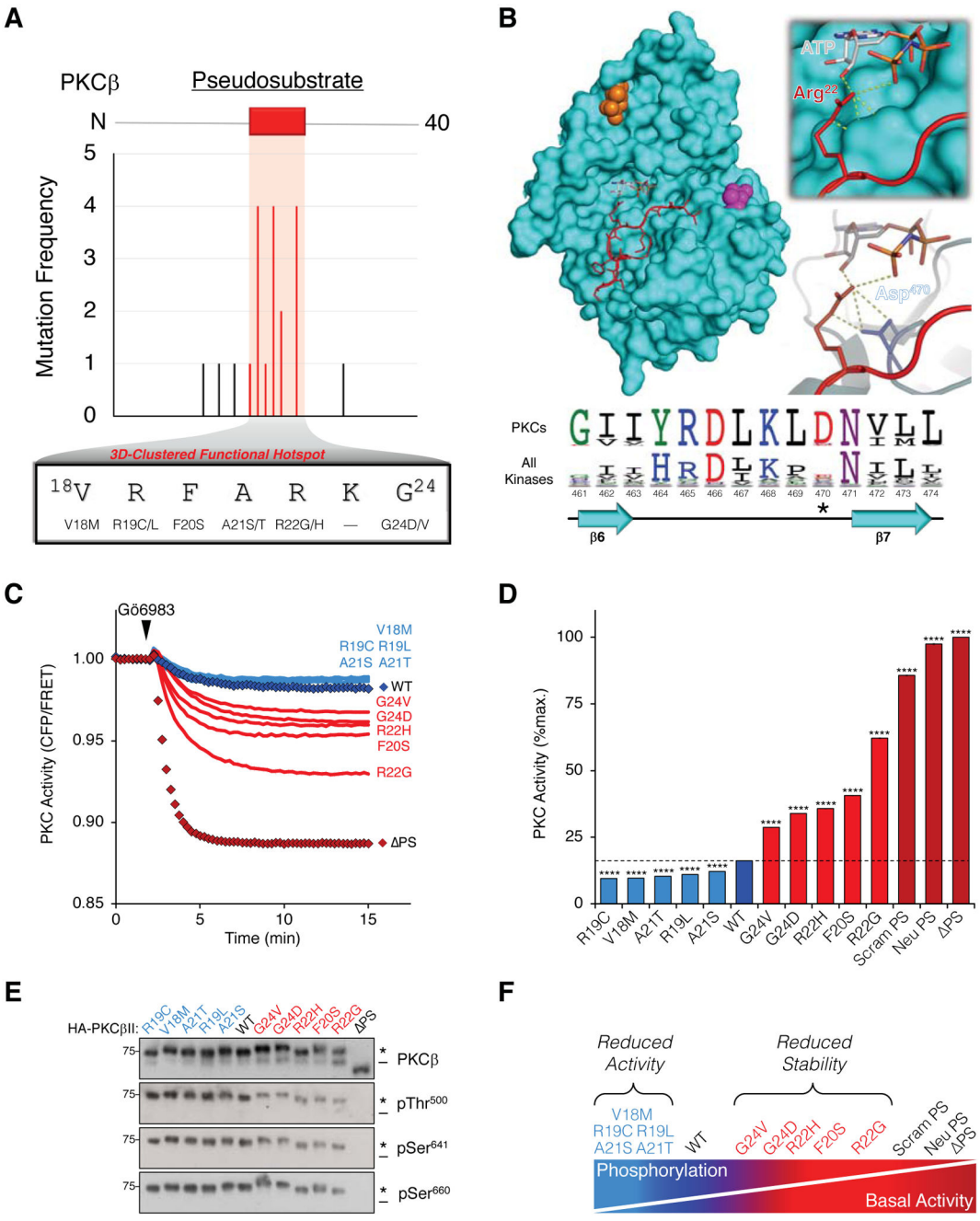

Figure 5. Cancer-Associated Pseudosubstrate Hotspot Mutations Reveal a Distinct PKC LOF Mechanism

(**A**) Mutations in the N-terminus (1-40) of PKCβ identified in human cancers showing 3D-clustered functional hotspot (red).

(**B**) Crystal structure of PKCβII with the pseudosubstrate modeled into the active site. Interactions between the pseudosubstrate (Arg^{22}), bound nucleotide (ATP), the kinase domain (Asp^{470}) are highlighted. KinView analysis showing evolutionary protein sequence conservation of the activation segment from all PKC isozymes (top) or all protein kinases (bottom). Height of the letter indicates the residue frequency at that position.

(**C**) COS7 cells co-expressing CKAR and indicated mCherry-PKCβII cancer-associated pseudosubstrate mutants were treated with Gö6983 (1μM) to determine basal activity.
(**D**) Quantification of (C) showing the magnitude of FRET ratio change upon inhibitor addition. Data represent three independent experiments of > 100 cells for each construct; dotted line indicates WT activity; ****$p < 0.0001$, by Repeated Measures One-Way ANOVA and Tukey-Kramer HSD test.
(**E**) IB analysis of lysates from COS7 cells expressing indicated PKC constructs probed with phospho-specific or total PKC antibodies.
(**F**) Schematic of cancer-associated pseudosubstrate mutants: pseudosubstrate mutations manifest as LOF, either by enhancing (Reduced Activity) or disrupting (Reduced Stability) PKC autoinhibition.

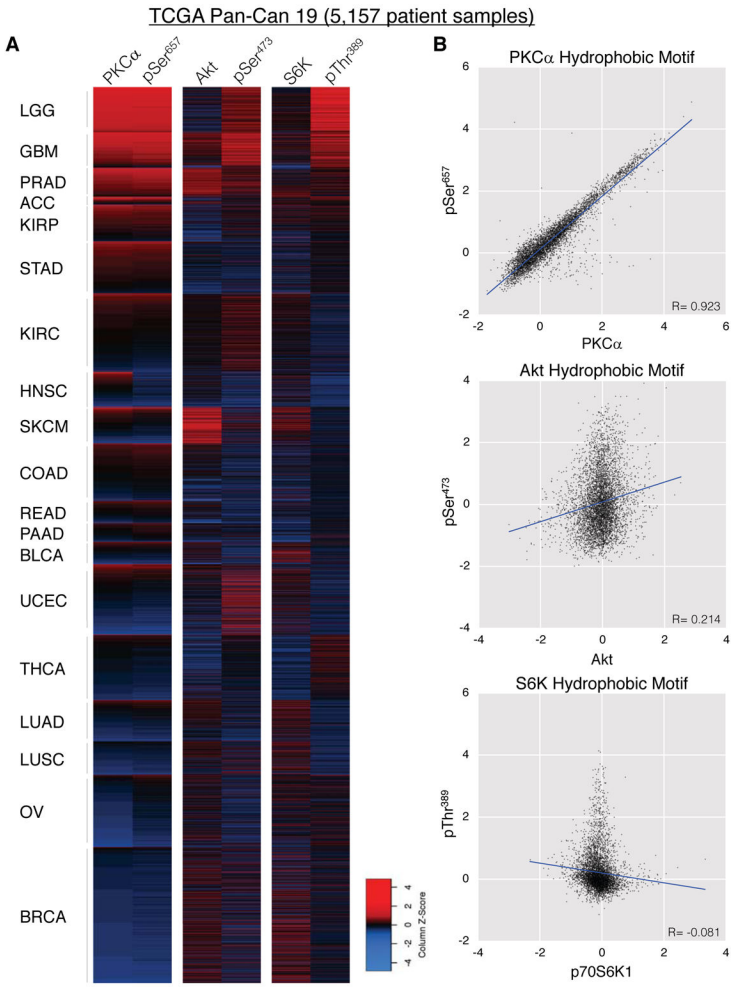

Figure 6. PKC Quality Control is Conserved in Human Cancer

(**A**) RPPA analysis of TCGA Pan Cancer Atlas tumor samples showing hydrophobic motif phosphorylation and total protein levels for PKC, Akt, or S6K. Cancer types are indicated by TCGA study abbreviations. (**B**) Quantification of (A): scatterplot of the expression of the indicated phosphorylation correlated with the associated total protein.

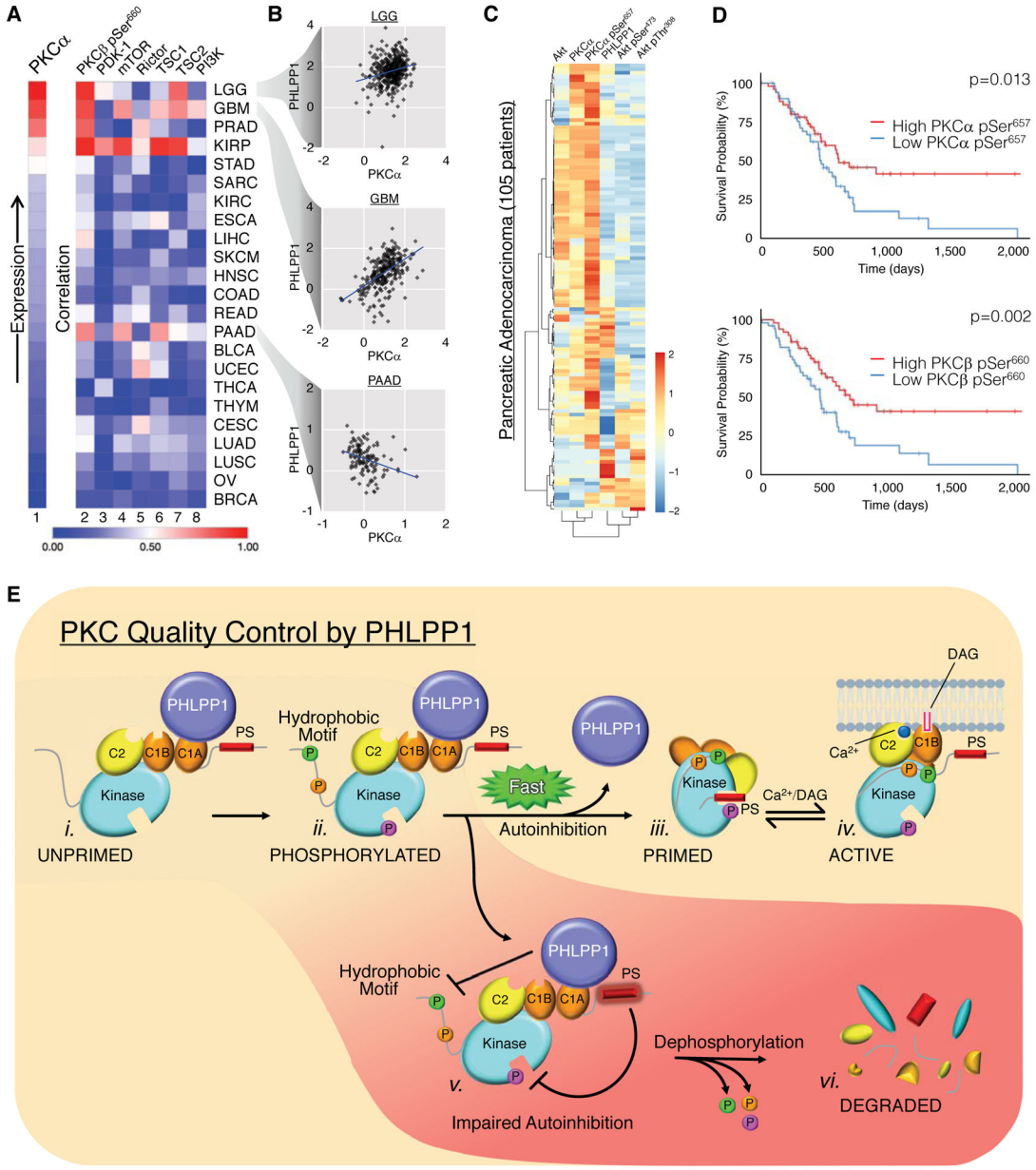

Figure 7. High PKC and Low PHLPP1 Levels are Protective in Pancreatic Adenocarcinoma.

(**A**) Heatmap of PKCα expression by cancer type (Expression; column 1). Heatmap showing coefficient of determination between PKCα hydrophobic motif phosphorylation and the indicated protein or phosphorylation (Correlation; columns 2-8). Cancer types are indicated by TCGA study abbreviations.

(**B**) RPPA analysis of PHLPP1 and PKCα levels in patient samples from the indicated cancers with Least-Squares Regression Line.

(**C**) Heatmap of individual PAAD patients showing relative abundance of the indicated protein or modification.

(**D**) Kaplan-Meier survival plots from PAAD patients stratified by PKC hydrophobic motif phosphorylation levels. p=log-rank p-value.

(**E**) Model of PKC Quality Control by PHLPP1: Newly-synthesized PKC (i) binds PHLPP1 where it surveys the conformation of this unprimed PKC to regulate phosphorylation of the hydrophobic motif. This species is in an open conformation, with the pseudosubstrate (PS; red rectangle) and all membrane-targeting modules unmasked. PKC that becomes phosphorylated (ii) is immediately autoinhibited, releasing PHLPP1 and entering the pool of stable, catalytically-competent but inactive enzyme (iii). This primed species is transiently and reversibly activated by binding second messengers (iv). PKC that does not properly autoinhibit following priming phosphorylations (v), for example due to mutations that impair autoinhibition, is rapidly dephosphorylated by PHLPP1 at the hydrophobic motif, leading to further dephosphorylation and degradation (vi).

KEY RESOURCES TABLE

REAGENT or RESOURCE	SOURCE	IDENTIFIER
Antibodies		
PKCα	BD Transduction	610108
PKCβ	BD Transduction	610128
PKCα/β pThr$^{497/500}$	Laboratory Stock	N/A
PKCα/β pThr$^{638/641}$	Cell Signaling Technologies	9375S
PKCα/β pSer$^{657/660}$	Cell Signaling Technologies	9371S
HA (Western Blot)	Roche	11867423001
HA (Immunoprecipitation)	BioLegend	901503
FLAG	BioLegend	637303
PHLPP1	Proteintech	22789-1-AP
Hsp90	Cell Signaling Technologies	610419
dsRED	Clonetech	632496
GST	Santa Cruz Biotechnology	sc-138
His	Sigma-Aldrich	H1029
α-Tubulin	Sigma-Aldrich	T6074
Chemicals		
Uridine-5-triphosphate (UTP)	Calbiochem	6701
Phorbol 12,13-dibutyrate (PDBu)	Calbiochem	524390-1MG
Gö6976	Calbiochem	365253
Gö6983	Calbiochem	80051-928
Bisindolylmaleimide IV (BisIV)	Calbiochem	203297
Cycloheximide (CHX)	Calbiochem	239764
Calyculin A	Cell Signaling Technologies	9902
DMSO	Sigma	D2650
Hank’s Balanced Salt Solution (HBSS)	Corning	21-022-CV
Phosphate-Buffered Saline (PBS)	Corning	21-031-CV
Dolbecco’s Modification of Eagle’s Medium F/12 (DMEM)	Corning	10-013-CV
Bis/Acrylamide Solution	Biorad	161-0156
PVDF	Biorad	162-0177
EXPRE^{35}S^{35}S Protein Labeling Mix	Perkin Elmer	NEG772007MC
Sf-900 II SFM	Gibco	10902-088
Penicillin/Streptomycin	Gibco	15140-122
Fetal Bovine Serum (FBS)	Atlanta Biologics	S11550 LOT#M15135
Trypsin-EDTA	Gibco	15400054
Triton X-100	Thermo Fisher Scientific	28314
Sodium Orthovanadate	NEB	P0758L
Leupeptin	Calbiochem	108975
Microcystin	Calbiochem	475815
PMSF	Calbiochem	80055-380
DTT	Sigma	10197777001

REAGENT or RESOURCE	SOURCE	IDENTIFIER
Critical Commercial Assays		
BCA Assay	Thermo Fisher Scientific	23225
SuperSignal West	Thermo Fisher Scientific	34078
Mini/Midi Prep Kit	Thermo Fisher Scientific	K210015
Pfu Turbo AD Polymerase	Agilent	600257
Q5 PCR	NEB	M0492L
T4 DNA Ligase	NEB	M0202L
Protein A/G Beads	Santa Cruz	sc-2003
Lipofectamine 3000	Thermo Fisher Scientific	L3000-075
Autoradiography Film	BioPioneer	MUBF-02
Cell Lines		
Cercopithecus aethiops kidney: COS-7	Laboratory Stock	ATCC-CRL-1651
Sf-9 Insect Cells	Laboratory Stock	ATCC PTA-3099
Phlpp1$^{+/+}$ *Mouse Embryonic Fibroblasts*	Laboratory Stock	(Chen et al., 2011)
Phlpp1$^{-/-}$ *Mouse Embryonic Fibroblasts*	Laboratory Stock	(Chen et al., 2011)
Recombinant DNA		
Plasmid: pcDNA3 CKAR	Laboratory Stock	N/A
Plasmid: pcDNA3 mCherry-rPKCβII	Laboratory Stock	N/A
Plasmid: pcDNA3 mCherry-rPKCβII ΔPS	Laboratory Stock	N/A
Plasmid: pcDNA3 mCherry-rPKCβII	Laboratory Stock	N/A
Plasmid: pcDNA3 mCherry-rPKCβII T500V	Laboratory Stock	N/A
Plasmid: pcDNA3 mCherry-rPKCβII T641A	Laboratory Stock	N/A
Plasmid: pcDNA3 mCherry-rPKCβII S660A	Laboratory Stock	N/A
Plasmid: pcDNA3 mCherry-rPKCβII T641E	Laboratory Stock	N/A
Plasmid: pcDNA3 mCherry-rPKCβII S660E	Laboratory Stock	N/A
Plasmid: pcDNA3 mCherry-rPKCβII T641E/S660E	Laboratory Stock	N/A
Plasmid: pcDNA3 mCherry-rPKCβII T641E/S660A	Laboratory Stock	N/A
Plasmid: pcDNA3 mCherry-hPKCα	Laboratory Stock	N/A
Plasmid: pcDNA3 mCherry-hPKCα ΔPS	Laboratory Stock	N/A
Plasmid: pcDNA3 mCherry-rPKCβII ΔPS	Laboratory Stock	N/A
Plasmid: pcDNA3 mCherry-rPKCβII ΔPS T641A	Laboratory Stock	N/A
Plasmid: pcDNA3 mCherry-rPKCβII ΔPS T641E	Laboratory Stock	N/A
Plasmid: pcDNA3 mCherry-rPKCβII ΔPS S660A	Laboratory Stock	N/A
Plasmid: pcDNA3 mCherry-rPKCβII ΔPS S660E	Laboratory Stock	N/A
Plasmid: pcDNA3 mCherry-rPKCβII ΔPS S660N	Laboratory Stock	N/A
Plasmid: pcDNA3 mCherry-rPKCβII Scrambled PS	Laboratory Stock	N/A
Plasmid: pcDNA3 mCherry-rPKCβII Neutral Pseudosubstrate	Laboratory Stock	N/A
Plasmid: pcDNA3 mCherry-hPKCβII	Laboratory Stock	N/A
Plasmid: pcDNA3 mCherry-hPKCβII Reg	Laboratory Stock	N/A
Plasmid: pcDNA3 mCherry-hPKCβII Reg ΔPS	Laboratory Stock	N/A
Plasmid: pcDNA3 mCherry-hPKCβII V18M	Laboratory Stock	N/A
Plasmid: pcDNA3 mCherry-hPKCβII R19C	Laboratory Stock	N/A

REAGENT or RESOURCE	SOURCE	IDENTIFIER
Plasmid: pcDNA3 mCherry-hPKCβII R19L	Laboratory Stock	N/A
Plasmid: pcDNA3 mCherry-hPKCβII F20S	Laboratory Stock	N/A
Plasmid: pcDNA3 mCherry-hPKCβII A21T	Laboratory Stock	N/A
Plasmid: pcDNA3 mCherry-hPKCβII A21S	Laboratory Stock	N/A
Plasmid: pcDNA3 mCherry-hPKCβII R22H	Laboratory Stock	N/A
Plasmid: pcDNA3 HA-hPKCβII	Laboratory Stock	N/A
Plasmid: pcDNA3 HA-hPKCβII ΔPS	Laboratory Stock	N/A
Plasmid: pcDNA3 HA-hPKCβII R22G	Laboratory Stock	N/A
Plasmid: pcDNA3 HA-hPKCβII G24V	Laboratory Stock	N/A
Plasmid: pcDNA3 HA-hPKCβII G24D	Laboratory Stock	N/A
Plasmid: pcDNA3 HA-hPKCβII V18M	Laboratory Stock	N/A
Plasmid: pcDNA3 HA-hPKCβII R19C	Laboratory Stock	N/A
Plasmid: pcDNA3 HA-hPKCβII R19L	Laboratory Stock	N/A
Plasmid: pcDNA3 HA -hPKCβII F20S	Laboratory Stock	N/A
Plasmid: pcDNA3 HA -hPKCβII A21T	Laboratory Stock	N/A
Plasmid: pcDNA3 HA -hPKCβII A21S	Laboratory Stock	N/A
Plasmid: pcDNA3 HA -hPKCβII R22H	Laboratory Stock	N/A
Plasmid: pcDNA3 HA -hPKCβII R22G	Laboratory Stock	N/A
Plasmid: pcDNA3 HA -hPKCβII G24V	Laboratory Stock	N/A
Plasmid: pcDNA3 HA -hPKCβII G24D	Laboratory Stock	N/A
Plasmid: pcDNA3 mCFP-rPKCβII-mYFP	Laboratory Stock	N/A
Plasmid: pcDNA3 mCFP-rPKCβII-mYFP K371R	Laboratory Stock	N/A
Plasmid: pcDNA3 mCFP-rPKCβII-mYFP Scrambled PS	Laboratory Stock	N/A
Plasmid: pcDNA3 mCFP-rPKCβII-mYFP Scrambled PS K371R	Laboratory Stock	N/A
Plasmid: pcDNA3 mCFP-rPKCβII-mYFP Neutral PS	Laboratory Stock	N/A
Plasmid: pcDNA3 mYFP-rPKCβII	Laboratory Stock	N/A
Plasmid: pcDNA3 mYFP-rPKCβII K371R	Laboratory Stock	N/A
Plasmid: pcDNA3 mYFP-rPKCβII Scrambled PS	Laboratory Stock	N/A
Plasmid: pcDNA3 mYFP-rPKCβII Neutral PS	Laboratory Stock	N/A
Plasmid: pcDNA3 Myristoylated-Palmitoylated mCFP	Laboratory Stock	N/A
Plasmid: pcDNA3 Golgi mCFP	Laboratory Stock	N/A
Plasmid: pcDNA3 FLAG-hPHLPP1	Laboratory Stock	N/A
Plasmid: pcDNA3 HA-rPKCβII	Laboratory Stock	N/A
Plasmid: pcDNA3 HA-rPKCβII K371R	Laboratory Stock	N/A
Plasmid: pcDNA3 HA-rPKCβII ΔPS	Laboratory Stock	N/A
Plasmid: pcDNA3 HA-rPKCβII Scrambled PS	Laboratory Stock	N/A
Plasmid: pcDNA3 HA-rPKCβII Neutral PS	Laboratory Stock	N/A
Plasmid: pcDNA3 HA-rPKCβII Catalytic Domain (296-673)	Laboratory Stock	N/A
Plasmid: pcDNA3 HA-rPKCβII ΔPS/C1A	Laboratory Stock	N/A
Plasmid: pcDNA3 HA-rPKCβII ΔPS/C1A/C1B	Laboratory Stock	N/A
Plasmid: pcDNA3 HA-rPKCβII ΔC2	Laboratory Stock	N/A

REAGENT or RESOURCE	SOURCE	IDENTIFIER
Plasmid: pcDNA3 HA-rPKCβII ΔC1A/C1B/C2	Laboratory Stock	N/A
Plasmid: pcDNA3 mCherry-rPKCβII ΔC1A	Laboratory Stock	N/A
Plasmid: pcDNA3 mCherry-rPKCβII ΔC2	Laboratory Stock	N/A
Plasmid: pcDNA3 mCherry-rPKCβII ΔC1B/C2	Laboratory Stock	N/A
Plasmid: pcDNA3 mCherry-rPKCβII ΔC1A/C1B/C2	Laboratory Stock	N/A
Plasmid: pcDNA3 mCherry-rPKCβII Cat	Laboratory Stock	N/A
Plasmid: pFastBac GST-hPHLPP1 PP2C	Laboratory Stock	N/A
Plasmid: pFastBac GST-hPKCβII	Laboratory Stock	N/A
Plasmid: pFastBac GST-hPKCβII ΔPS (Δ19-36)	Laboratory Stock	N/A
Software		
Metafluor	Molecular Devices	https:/www.moleculardevices.com/products/cellular-imaging-systems
Image J	NIH	https://imagej.nih.gov/ij/
AlphaView for FluorChem Q	Protein Simple	https://proteinsimple.com/software_alphaview.htm#fluorocehm
Prism 6	Graphpad	https://www.graphpad.com/scientific-software/prism/